In: Monomers, Oligomers, Polymers, Composites… ISBN: 978-1-60456-877-6
Editors: R. A. Pethrick, G.E. Zaikov et al.

Chapter 4

FEATURES OF MECHANISM OF FREE RADICAL INITIATION IN POLYMERS UNDER EXPOSURE TO NITROGEN OXIDES

E. Ya. Davydov, I. S. Gaponova, T. V. Pokholok, G. B. Pariyskii and G. E. Zaikov
Emanuel Institute of Biochemical Physics, Russian Academy of Sciences.
4 Kosygin Street. 119334 Moscow, Russia
Fax: (495) 939-71-03, E-mail: *pgb@sky.chph.ras.ru*

ABSTRACT

The mechanism of interactions of NO, NO_2, NO_3 as well as dimers of NO_2 with functional groups of organic molecules and polymers are considered. It is demonstrated that nitrogen oxides are active initiators of radical reactions as a result of which various molecular products of nitration and stable nitrogen-containing radicals are formed. Features of the initiation mechanism determining the composition of molecular and radical products of conversions of the compounds on exposure to nitrogen oxides have been revealed.

Keywords: nitrogen oxides, polymers, macroradicals, EPR spectra, mechanism of reactions

I. INTRODUCTION

Nitrogen oxides play the important role in various chemical processes proceeding in an atmosphere, and affect on an environment[1-4]. These compounds ejected to atmosphere by the factories and transport in huge amounts creates thus serious problems for fauna and flora as well as synthetic polymeric materials. In this connection, the researches of the mechanism of nitrogen oxide reactions with various organic compounds including polymers are important for definition of stability of these materials in polluted atmosphere. On the other hand, these researches can be used in synthetic chemistry[5-7], in particular for development of methods

of the polymer modification, for example, for preparation of spin-labelled macromolecules[8,9]. The generation of spin labels occurs thus in consecutive reactions including formation and conversion of specific intermediate molecular products and active free radicals. It is necessary to note essential advantages of such way of obtaining spin labels not requiring application of complex synthetic methods based on reactions of stable nitroxyl radicals with functional groups of macroradicals[10]. If the polymers are capable of reacting with nitrogen oxides, the formation of stable radicals in them takes place spontaneously or by thermolysis of molecular products of nitration[11,12].

Most important for reactions with various organic compounds and polymers are nitrogen oxides of the three types: NO, NO_2, NO_3. All of them represent free radicals with different reactivity[13]. In the present review the features of the mechanism of reactions of these oxides and also NO_2 dimeric forms with a number of polymers and low-molecular compounds are considered. The especial attention is given to the analysis of structure of stable nitrogen-containing radicals and kinetic features of their formation. On the basis of results of the analysis, the conclusions on the mechanism of primary reactions of initiation and intermediate stages of complex radical processes under action of nitrogen oxides are given. The principles of use of nitrogen oxides for grafting spin labels to various polymers are considered.

II. INTERACTION OF NITROGEN OXIDES WITH PRODUCTS OF PHOTOLYSIS AND RADIOLYSIS OF POLYMERS

From three nitrogen oxides examined, the radical NO is least reactive. It is not capable of abstracting hydrogen atoms even from least strong tertiary or allyl C–H bonds; the strength of H–NO bond[14] makes only 205 kJ·mol^{-1}. Nitrogen oxide cannot join to isolated double C=C bonds of alkenes[15]. For NO, the recombination with free radicals with formation of effective spin traps (nitroso compounds) is characteristic process. The structure of stable nitrogen-containing radicals formed from nitroso compounds in the subsequent reactions gives information on the mechanism of proceeding radical process in the given reacting system.

During photolysis of polymethylmethacrylate (PMMA) in atmosphere of NO by unfiltered light of a mercury lamp at 298 K, the formation of acylalkylaminoxyl radicals such as $R_1N(O^{\bullet})C(=O)OR_2$ was observed with typical parameters of anisotropic triplet EPR spectrum in a solid phase[16]: $A_{II}^{N} = 2.1 \pm 0.1$ mT and g_{II}=2.0027 ± 0.0005. If photolysis of the same samples to carry out at 383 K, dialkylaminoxyl radicals $RN(O^{\bullet})R$ in addition to acylalkylaminoxyl radicals are formed with parameters of EPR spectrum: $A_{II}^{N} = 3.2 \pm 0.1$ mT and g_{II}=2.0026 ± 0.0005. Under action of filtered UV light (260-400 nm) at room temperature there is a third type of stable radicals namely iminoxyls $(R_1R_2)C=NO^{\bullet}$, the triplet EPR spectrum of which in benzene solution of PMMA is characterized by the parameters: a^N = 2.8 mT and g = 2.005. The occurrence of acylalkylaminoxyl radicals is evidence of eliminating of methoxycarbonyl radicals in a course of the polymer photolysis:

$$\sim(CH_3)C(COOCH_3)CH_2(CH_3)C(COOCH_3)\sim \xrightarrow{h\nu}$$
$$\sim(CH_3)C(COOCH_3)CH_2C^{\bullet}(CH_3)\sim (R^{\bullet}) + {}^{\bullet}COOCH_3 \quad (1)$$

The subsequent reaction with participation of NO gives acylalkylaminoxyl radicals:

$${}^{\bullet}COOCH_3 + NO \rightarrow O{=}N{-}COOCH_3 \xrightarrow{+R^{\bullet}} RN(O^{\bullet})COOCH_3 \quad (2)$$

Dialkylaminoxyl radicals are formed by decomposition of macroradicals $R^{\bullet}$:

$$R^{\bullet} \xrightarrow{kT} \sim(CH_3)C(COOCH_3)CH_2{=}C(CH_3)CH_2\sim + {}^{\bullet}C(CH_3)(COOCH_3)\sim$$
$$\xrightarrow{+NO,R^{\bullet}}$$
$$RN(O^{\bullet})C(CH_3)(COOCH_3)\sim \quad (3)$$

Iminoxyl radicals are appeared as a result of generation of macroradicals $\sim(CH_3)C(COOCH_3)C^{\bullet}H(CH_3)C(COOCH_3)\sim$ ($R_1^{\bullet}$) which in NO atmosphere are converted into nitroso compounds and further into oximes:

$$R_1^{\bullet} + NO \rightarrow R_1NO \rightarrow \sim(CH_3)C(COOCH_3)C(=NOH)(CH_3)C(COOCH_3)\sim(R_1R_2NOH) \quad (4)$$

As a result of the mobile hydrogen atom abstraction from oximes by, for example, methoxycarbonyl radical, iminoxyls are formed:

$$R_1R_2NOH + {}^{\bullet}COOCH_3 \rightarrow HCOOCH_3 + R_1R_2NO^{\bullet} \quad (5)$$

A limiting stage of reaction (2) is nitrogen oxide diffusion in a polymeric matrix. The rate of reaction (3) should much more depend on mobility of macromolecular reagents. Therefore, the distinction in composition of radicals in PMMA photolysed at room temperature and 383 K is observed. At room temperature, acylalkylaminoxyl radicals are formed due to accepting low-molecular methoxycarbonyl radicals ${}^{\bullet}COOCH_3$ by nitroso compounds. At 383K, when molecular mobility essentially grows, dialkylaminoxyl radicals $R_1N(O^{\bullet})R_2$ are formed because the meeting two macromolecular particles is provided. The results obtained demonstrate an opportunity of NO use for an elucidation of the polymer photolysis mechanism. With the help of this reactant, it was possible to establish a nature and mechanism of formation of intermediate short-lived radicals in photochemical process using EPR spectra of stable aminoxy radicals.

The application of nitrogen oxide enables to prepare spin-labelled macromolecules in chemically inert and insoluble polymers, for example, in polyperfluoroalkanes. As was shown in the work[16], the radiolysis of oriented films of polytetrafluoroethylene (PTFE) and copolymer of tetrafluoroethylene with hexafluoropropylene initiates reactions with formation of iminoxyl macroradical according to the following scheme:

$$\text{PTFE} \xrightarrow{\gamma} \sim CF_2C^{\bullet}FCF_2 \sim + NO \rightarrow \sim CF_2CF(NO)CF_2 \sim \xrightarrow{\gamma}$$
$$\sim CF_2C^{\bullet}(NO)CF_2 \sim \rightarrow \sim CF_2C(=NO^{\bullet})CF_2 \sim \quad (6)$$

$$\sim CF_2CF(CF_3)CF_2 \sim \xrightarrow{\gamma, NO} \sim CF_2CF(CF_2NO)CF_2 \sim \xrightarrow{\gamma}$$
$$\sim CF_2CF(C^{\bullet}FNO)CF_2 \sim \rightarrow \sim CF_2CF(CF=NO^{\bullet})CF_2 \sim \quad (7)$$

The EPR spectrum of iminoxyl radicals in oriented PTFE films represents a triplet (A_{II}^{N} =4.1 ± 0.1mT) of septets (A_{II}^{F} = 0.5 ±0.1 mT) with g_{II} =2.0029 ±0.0005. The unpaired electron in fluoroiminoxyl radicals interacts with a nitrogen nucleus and four in pairs magnetically equivalent fluorine nucleuses with hyperfine splittings of 1.0 ± 0.1 and 0.5 ± 0.1 mT.

Aminoxyl radicals in polyperfluoroalkanes are not formed in these conditions. However, if to carry out a preliminary γ–irradiation on air, middle and end peroxide macroradicals appear with conversion into fluoroaminoxyl macroradicals ~ $CF_2CF(NO^{\bullet})CF_2$ ~ by the subsequent exposure to NO. Their EPR spectra in oriented films are quintet of triplets with the parameters: A_{II}^{N} =0.46 mT, A_{II}^{F} =1.11 mT, g_{II} =2.006; $A_{\perp}^{N}$ =1.12 mT, $A_{\perp}^{F}$ =1.61 mT and $g_{\perp}$ =2,0071. The following mechanism of formation of aminoxyl radicals in these conditions is offered[17]:

$$\sim CF_2\,CF_2\,C^{\bullet}F\,CF_2 \sim \rightarrow \sim C^{\bullet}F_2 + CF_2{=}CFCF_2{\sim} \quad (8)$$

The end alkyl radical is oxidized into end peroxide radical:

$$\sim C^{\bullet}F_2 + O_2 \rightarrow \sim CF_2OO^{\bullet} \quad (9)$$

In NO atmosphere, end peroxide radical is converted as follows:

$$\sim CF_2CF_2OO^{\bullet} + NO \rightarrow \sim CF_2CF_2O^{\bullet} + NO_2 \quad (10)$$

$$\sim CF_2CF_2O^{\bullet} + NO{\sim} \leftrightarrow CF_2CF_2ONO \quad (11)$$

$$\sim CF_2CF_2O^{\bullet} \rightarrow \sim C^{\bullet}F_2 + COF_2 \quad (12)$$

$$\sim C^{\bullet}F_2 + NO \rightarrow \sim CF_2NO \quad (13)$$

$$\sim CF_2NO + CF_2{=}CFCF_2{\sim} \xrightarrow{NO} {\sim}CF_2N(O^{\bullet})CF_2CF(NO)CF_2{\sim} \quad (14)$$

In copolymer of tetrafluoroethylene with hexafluoropropylene, the radicals ~$CF_2N(O^{\bullet})CF_3$ are formed in the same conditions[17].

Thus, spin-labelled macromolecules of fluoroalkyl polymers can be prepared using postradiational free radical reactions in NO atmosphere. The advantage of this method of

introduction of spin labels lies in the fact that the radical centre can be located both in the end and in middle of macrochains, that allows basically to obtain the optimum information on molecular dynamics.

III. RADICAL REACTIONS INITIATED BY NITROGEN TRIOXIDE

The radicals NO_3 play an essential role in chemical processes proceeding in the top layers of atmosphere[18]. These radicals are formed in reaction of nitrogen dioxide with ozone:

$$NO_2 + O_3 \rightarrow NO_3 + O_2 \qquad (15)$$

Under action of daylight, nitrogen trioxide is consumed with releasing atomic oxygen:

$$NO_3 \xrightarrow{h\nu} NO_2 + O \qquad (16)$$

Its disappearance occurs at night in reaction with nitrogen dioxide too:

$$NO_3 + NO_2 \rightarrow N_2O_5 \qquad (17)$$

The NO^3 radicals are characterized by high reactivity in reactions with various organic compounds[18-22]. Typical reactions of these radicals are abstraction of hydrogen atoms from C–H and addition to double bonds. Along with these reactions, the radicals NO_3 are decomposed in thermal and photochemical processes. The thermal decomposition of nitrogen trioxide generated by pulse radiolysis of concentrated water solutions of a nitric acid takes place with high rate ($k_{208K} = 8 \cdot 10^{3}$, s^{-1})[23]:

$$NO_3 \xrightarrow{kT} NO_2 + O \qquad (18)$$

The radicals NO_3 have three intensive bands of absorption in visible region of an optical spectrum with λ_{max} = 600, 640 и 675 nm, and in UV region at 340–360 nm[18,19,23-27]. The action of light on NO_3 results in dissociation of them by two mechanisms including formation of NO_2 and atomic oxygen similarly to reaction (18) or nitrogen oxide and molecular oxygen[1]:

$$NO_3 \rightarrow NO + O_2 \qquad (19)$$

The efficiency of the NO_3 conversion by one or either mechanisms is determined by spectral composition of light. The approximate border of wave lengths for photodissociation by reactions (18) or (19) lays at 570 nm. Above 570 nm, NO_3 decomposes on NO and O_2 with the very high (~ 1) quantum yield; the basic products of the photolysis are NO_2 + O below 570 nm [1].

One of the most widely widespread ways of the NO_3 generation is the photolysis of Ce (IV) nitrates in particular ceric ammonium nitrate (CAN) $(NH_4)_2Ce(NO_3)_6$. The absorption

spectrum of CAN has a wide and intensive band with a maximum at 305 nm (ε = 5890 l·mol^{-1}·см$^{-1}$) which is conditioned by an electron transfer to $Ce^{4+}$from nitrate anion[26]. Under action of light in the given spectral region there is a photoreduction of CAN [26,27]:

$$Ce^{4+}NO_3^- \rightarrow Ce^{3+} + NO_3 \qquad (20)$$

Thus, the CAN photolysis gives different active radical particles: NO, NO_2, NO_3 and atomic oxygen. Use of light of various spectral composition allows thus to generate these particles in different ratio.

Atomic oxygen being very active reactant [14] interacts with C─H bonds of organic compounds. Macroradicals formed by action of atoms O on polymers can be converted in the presence of NO into stable aminoxyl radicals. The possibility using these processes for the purposes of chemical modification of polymers is considered by the example of polyvinylpyrrolidone (PVP) in the works [28,29] In PVP with CAN (0,05─0,2 mol kg^{-1}) in the course of photolysis by light with $\lambda > 280$ nm, the formation of alkyl macroradicals is registered by EPR as a result of the reaction:

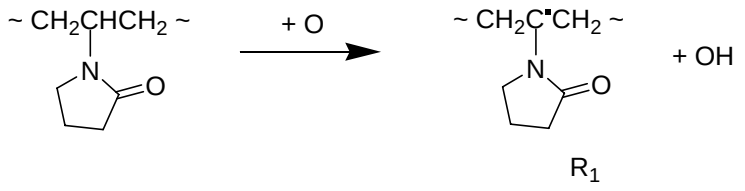

(21)

The radicals R_1 are stabilized only at low temperatures (77 K). Photolysis of samples at 298 K by the same light results in the production of stable dialkylaminoxyl radicals characterized by anisotropic EPR triplet spectrum with parameters of A_{II}^{N} = 3.18 mT and g_{II} = 2.0024. The cross-linkage of PVP macromolecules takes place in these conditions with formation of a gel-fraction as a result recombination of macroradicals R_1 with nitrogen oxide:

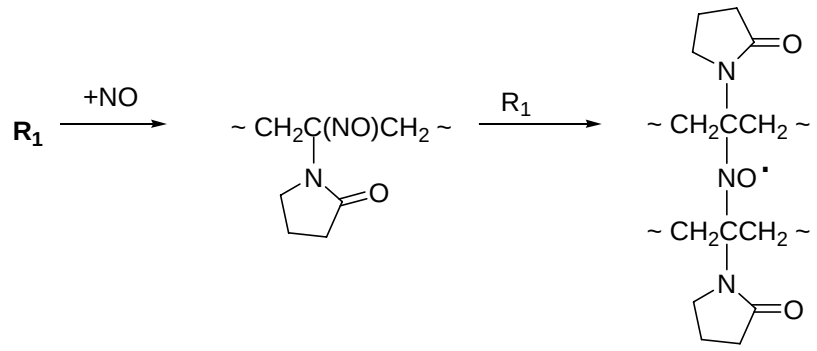

(22)

As shown in the work [28], the yield of a gel-fraction directly correlates with the amounts of stable radicals which in the given system represent cross-linkages of macromolecules.

Such simple method of cross-linking PVP can be applied for obtaining hydrogels used as specific sorbents [30].

IV. FREE RADICAL AND ION - RADICAL REACTIONS UNDER ACTION OF NITROGEN DIOXIDE AND ITS DIMERS

Nitrogen dioxide effectively reacts with various low- and high-molecular organic compounds [5-7, 31]. However it must be emphasized that NO_2 is a free radical of moderate reactivity, and the ONO─H bond strength [14] makes up 320 kJ mol^{-1}. Therefore radicals NO_2 are capable of initiating free radical reactions by abstraction of hydrogen atoms from least strong, for example, allyl C─H bonds or addition to double C=C bonds [32,33]:

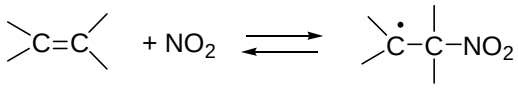

(23)

This process causes further radical conversions of olefins with formation of dinitro compounds and nitro nitrites:

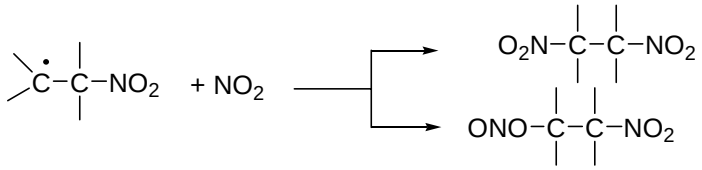

(24,25)

From Jellinek's data [31], butyl rubber destroys under the action of NO_2:

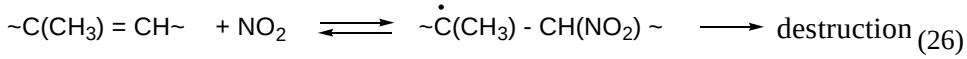

(26)

As a consequence of primary reactions of nitrogen dioxide radicals with the isolated double bonds, stable aminoxyl radicals can be generated. Such transformations are characteristic for rubbers.

IV.1. Preparation of Spin-Labelled Rubbers

The possibility of obtaining spin-labelled rubbers by interaction of their solutions in the inert solvents with a mixture of nitrogen dioxide and oxygen has been demonstrated in the work [34]. Such rubbers can be prepared simply and rapidly by reactions of block polymeric samples with gaseous NO_2 [35]. The experiments were carried on 1,4-*cis*-polyisoprene (PI) and copolymer of ethylene, propylene and dicyclopentadiene. The samples had the form of cylinders of 1.5 cm height and 0.4 cm in diameter. On exposure these polymers to NO_2 (10^{-5}–$2.3 \cdot 10^{-3}$ mol·l^{-1}) at 293 K, identical EPR spectra were registered. The spectra represent an

anisotropic triplet with parameters which are typical for dialkylaminoxyl radicals with A_{II}^{N} = 3.1 mT and g_{II} = 2.0028 ± 0.0005. The spectra with such parameters testify that the correlation time of rotational mobility τ_c at the given temperature exceeds 10^{-9} s. At increasing temperature up to 373 K, the isotropic triplet signal with a^{N} = 1.53 ± 0.03 mT and g = 2.0057 ± 0.0005 was observed, that is caused by essential decreasing correlation time ($5\cdot10^{-11} < \tau_c < 10^{-9}$ s). The change of τ_c with temperature is described by the relation $\tau_c = \tau_0 \exp(E/RT)$, where $\log \tau_0 = -14.2$, and E is the activation energy of rotational diffusion (34.7 kJ·mol^{-1})

The study of kinetics of the aminoxyl radical accumulation has shown that concentrations of the radicals pass through a maximum determined by concentrations of NO_2 in a gas phase. So the concentration of radicals peaks in 40 times time more slowly when [NO_2] falls from $2.3\cdot10^{-3}$ up to 10^{-5} mol·l^{-1}. It is suggested that such kinetic features are due to disappearance of aminoxyl radicals in reactions of their oxidation by NO_2 dimers. The presence of oxygen in a gas mixture results in the long induction period for kinetics of the radical formation, however their maximum concentration in this case are approximately in 3 times higher than on exposure of rubbers to pure NO_2. The scheme of the aminoxyl radical formation includes four basic stages: generation of macroradicals in reaction of NO_2 with rubbers; synthesis of macromolecular, spin trapping of macroradicals by nitroso compounds, and destruction of aminoxyl radicals:

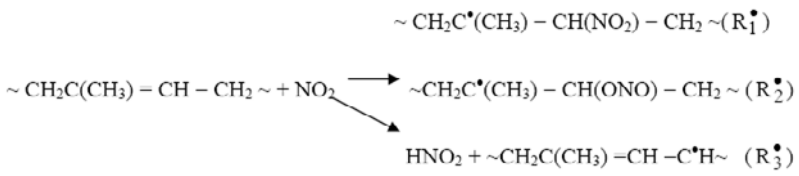

(27)

$R_1^{\bullet}(R_2^{\bullet}, R_3^{\bullet}) + NO_2 \rightarrow$ продукты (28)

$2HNO_2 \rightleftharpoons NO + NO_2 + H_2O$ (29)

$R_1^{\bullet}(R_2^{\bullet}, R_3^{\bullet}) + NO \rightarrow R_1NO(R_2NO, R_3NO)$ (30)

$RNO + R_1^{\bullet}(R_2^{\bullet}, R_3^{\bullet}) \rightarrow (R)_2N{-}O^{\bullet}$ (31)

$(R)_2N{-}O^{\bullet} + R^{\bullet} \rightarrow (R)_2N{-}OR$ (32)

$(R)_2N{-}O^{\bullet} + N_2O_4 \rightarrow [(R)_2N^{+}ONO_3^{-}] + NO$ (33)

As can be seen from this scheme, the accumulation of aminoxyl radicals should be accompanied by cross-linkage of macromolecules. The presence of oxygen inhibits the aminoxyl accumulation as a result of conversions of primary nitroalkyl and allyl macroradicals into peroxide radicals.

In the course of interaction of solid polymers with NO_2 one can expect a non-uniform distribution of formed stable nitrogen-containing radicals in sample owing to diffusion

restrictions. A possibility of an examination of the nitration reaction front thus is created in polymeric materials by measurement of spatial distribution of aminoxyl radicals. Such studies can be performed using the method of EPR tomography (or the EPR imaging technique) described in the works [36,37]. During the reaction of NO_2 with double bonds of rubbers, the spatial distribution of aminoxyls characterizes kinetics of the reaction front progress and thus structural - physical properties of a concrete sample. The EPR tomograms in a non-uniform magnetic field (figures 1a and b) were obtained for cylindrical samples PI of 0.4 cm in diameter and height of 1.5 cm. The accumulation of aminoxyl macroradicals up to maximum concentrations in enough thick layers (~1 mm) of samples shows that a spatial grid of cross-linked PI hindered diffusion of NO_2 has not time to be generated. The introduction of O_2 in gaseous mixture narrows front of reaction and reduces rate of the aminoxyl radical formation. This effect is connected with the additional channel of an intensive consumption of intermediate macroradicals $R_1^{\bullet}$ ($R_2^{\bullet}$, $R_3^{\bullet}$) and decreasing their equilibrium concentration. The results obtained by EPR tomography have shown that on exposure of rubbers to NO_2 at enough high concentrations (10^{-4} – $2{,}3\cdot10^{-3}$ mol·l^{-1}) the chemical and structural modification occurs in a superficial layer and does not take place in deeper layers.

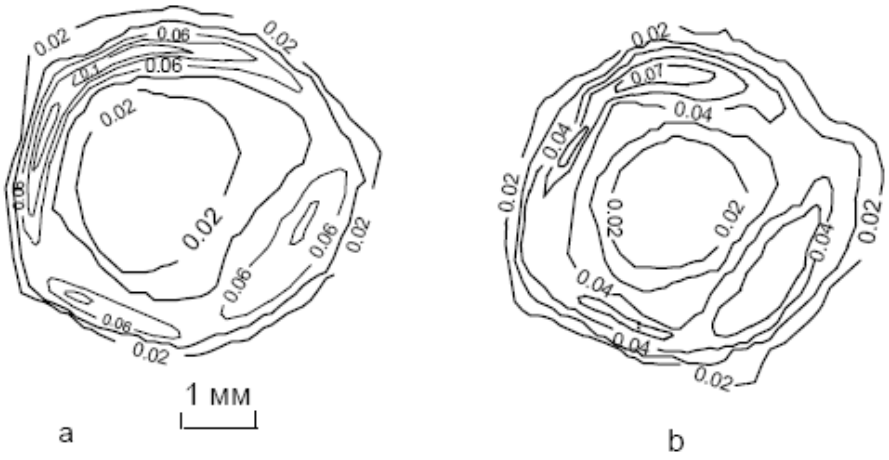

Figure 1. Bulk distribution of dialkylaminoxyl radicals produced upon nitration of PI by NO_2 during 2.5 (a) and 740 hours (b).

V. On the Mechanism of Initiation of Radical Reactions by Nitrogen Dioxide Dimers

As noted above, nitrogen dioxide can initiate free radical reaction in compounds containing least strong C─H bonds or double C=C bonds. However, the effective formation of stable nitrogen-containing radicals was observed also in aromatic polyamidoimides, polycaproamide, polyvinylpyrrolidone (PVP)[8] and also aromatic polyamide (AP) [12]. These facts allow considering other probable mechanisms of the radical processes initiation. The fact is that the basic radical products of interaction of nitrogen oxide with polymers containing amide groups are iminoxyl and acylalkylaminoxyl radicals which are produced

from oximes and acylnitroso compounds [8,12]. The occurrence of these predecessors of stable radicals is in turn connected with the nitrogen oxide formation.

In this connection, it is necessary to suppose a participation of NO_2 dimeric forms in radical initiation. The main dimers of NO_2 are planar nitrogen tetroxide $O_2N\text{-}NO_2$ (PD) and nitrosyl nitrate $ONONO_2$ (NN). Ab initio calculations [33] show that these dimers are formed with the most probability in NO_2 atmosphere; the form of nitrosyl peroxynitrite ONOONO is too unstable to be considered as efficient participant of reactions, however it can play a role of intermediate compound at oxidation of nitrogen oxide by oxygen [38]. As NN has strong oxidative properties [39], the generation of radicals can take place by an electron transfer from donor functional groups with the formation of intermediate radical cations [9,40]:

$$RH + ONONO_2 \rightarrow [R^{\bullet}H^{+}(NO\cdots ONO_2^{-})] \rightarrow R^{\bullet} + NO + H^{+} + ONO_2^{-} \qquad (36)$$

The recombination of radicals with nitric oxide gives nitroso compounds that undergo isomerisation into oximes [41] to produce iminoxyl radicals in the reaction with NO_2:

$$\diagdown\!\!\diagup C{=}NOH + NO_2 \rightarrow \diagdown\!\!\diagup C{=}NO^{\bullet} + HNO_2 \qquad (37)$$

The tertiary nitroso compounds are effective spin traps and a source of stable aminoxyl radicals:

$$RN{=}O + R_1^{\bullet} \rightarrow R(R_1)N\text{-}O^{\bullet} \qquad (38)$$

Thus the mechanism involving reactions (36-38) formally could explain an appearance of stable radicals in the polymers not containing specific chemical bonds reacting with NO_2 mono radicals. However, there are certain obstacles connected with energetic properties of NO_2 dimers [33] for realizing such mechanism; the energy of syn- and anti forms of NN exceeds that of PD respectively 29.8 and 18.4 кJ·mol^{-1}; that is the equilibrium

$$O_2N\text{-}NO_2 \rightleftharpoons 2NO_2 \rightleftharpoons ONONO_2 \qquad (39)$$

should be shifted to PD in gas phase.

The diamagnetic (PD) is capable of generating nitrogen-containing radicals in specific reaction with system of the connected double bonds of *p* ─ quinines (Q) [42]. On exposure of BQ to nitrogen dioxide, the formation of radicals I of oxyaminoxyl type (R_{oxy}) [43] takes place by the following scheme:

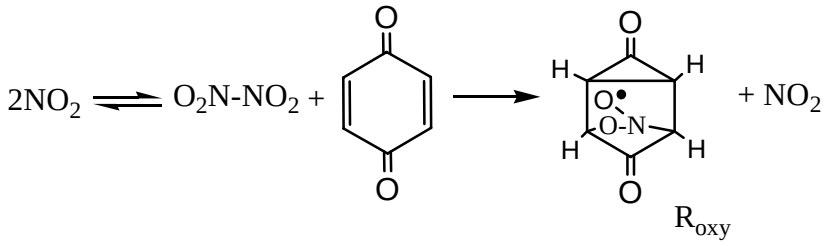

(40)

The triplet EPR spectrum of radicals R_{oxy} in Q (figure 2a) has parameters: a^N = 2.82 mT and g = 2.0053. The scheme (40) is confirmed by kinetic data according to which the rate of the radical accumulation is proportional to a square of NO_2 concentration in gas phase.

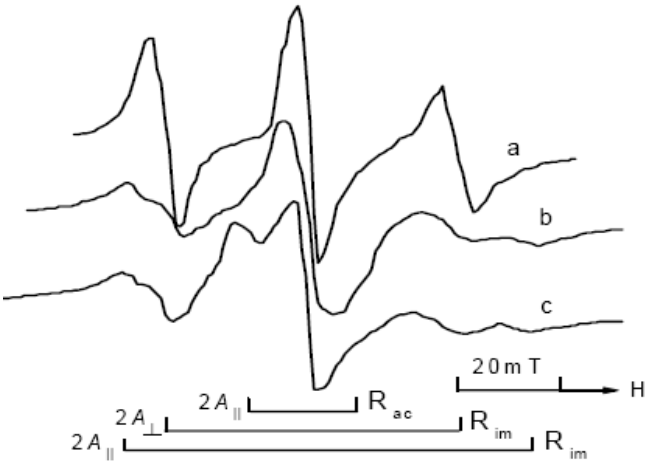

Figure 2. EPR spectra of Q after exposure to NO_2 (a); Q + AP (b) and Q+ PVP (c) after preliminary exposure to NO_2 and subsequent pumping-out the composites.

Thus, both dimer forms of NO_2 can be active. On this basis it is possible to suggest that the shift of equilibrium (39) to the formation of NN in PVP and AP is caused by specific donor-acceptor interaction of PD with amide groups which induce the conversion into NN and ion - radical process by scheme (36). As the indicator of conversion of PD into NN, the dependence of a yield of radicals R_{oxy} on the contents of AP and PVP was used in composites: Q + AP and Q + PVP. To increase a surface of interaction with nitrogen dioxide, silica gel with particles of 100-160 μ in diameter was added to the composites. Samples for measurement of EPR spectra contained constant quantities of Q (100 mg), SiO_2 (100 mg) and variable quantities of PVP (10-30 mg) or AP (10-50 mg). In addition to R_{oxy}**,** iminoxyl radicals R_{im} [8] occur in composites of BQ with AP on exposure to nitrogen dioxide. Under the same conditions, the sum of radicals R_{im} and acylalkylaminoxyl radicals R_{ac}**,** [8] along with R_{oxy}**,** was registered in composites of BQ with PVP. Signals of radicals R_{im} and R_{ac} are masked by an intense signal of radicals R_{oxy} in the EPR spectrum. However on can separate spectra of radicals R_{im} and R_{ac} using the fact that radicals R_{oxy} exist only in NO_2 atmosphere. In view of rather low thermal stability, radicals R_{oxy} quickly disappear at room temperature within several minutes after pumping out nitrogen dioxide from the samples. Remaining spectra of stable radicals R_{im} in AP and the sum of R_{im}+R_{ac} in PVP are shown respectively in

figures 2b and 2c. They represent anisotropic triplets with $A_{||}^{N}$ = 4.1 mT, $g_{||}$ = 2.0024 and $A_{\perp}^{N}$ = 2.6 mT, $g_{\perp}$ = 2.005 (R_{im}) [12] and with $A_{||}^{N}$ = 1.94 mT, $g_{||}$ = 2.003 (R_{ac}) [8]. Using this procedure, the maximum concentrations of radicals R_{oxy}, R_{im} and R_{ac} were separately determined in composites with the various contents of AP and PVP after exposure to NO_2 within 24 hours. The results obtained are shown in figures 3a and 3b. As is seen from the figures, the concentration of radicals R_{oxy} accumulated monotonously falls as the relative contents of AP and PVP is increased, while concentrations of radicals R_{im} and R_{im} + R_{ac} vary within 10 - 20 % of the average value, that is within the accuracy of integration of EPR spectra. This fact is indicative of obvious dependence of the radical R_{oxy} yield on the contents of polymers with amide groups in composites, suggesting that PD is converted under the influence of amide groups into NN that generates stable radicals R_{im} and R_{ac} in the polymeric phases. It is significant that an appreciable decrease of the yield of radicals R_{oxy} was not observed in control experiments when polymers of other chemical structure, for example, acetyl cellulose were used in composites. Therefore one can conclude that amide groups play special role in the process PD $\rightarrow$ NN.

The scheme of R_{im} formation in AP can be presented as follows:

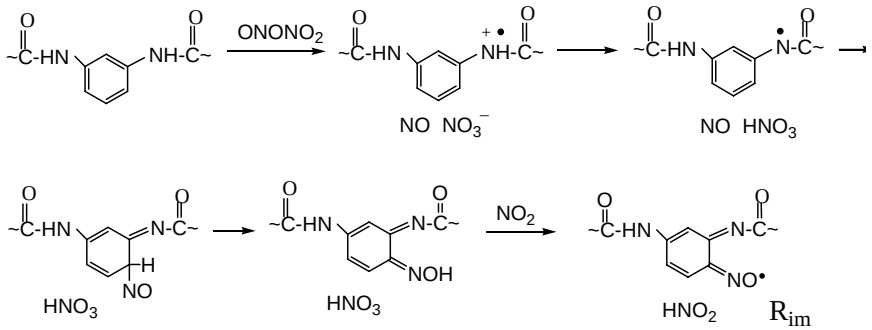

(41)

The structure of radicals R_{im} in AP is confirmed by quantum-chemical calculations of HFI constants [12].

The formation of radicals R_{im} and R_{ac} in PVP can be described by the following reactions:

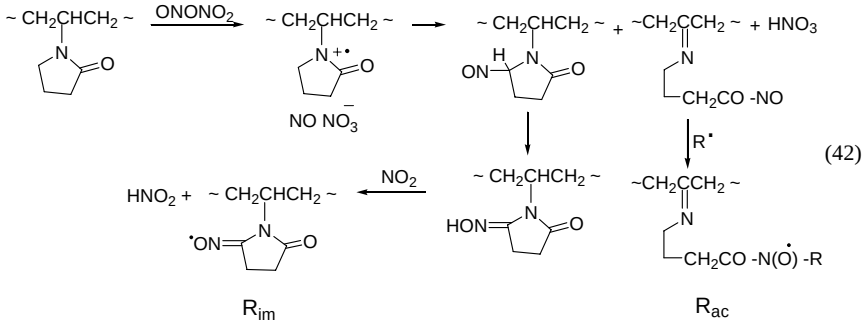

(42)

where $R^{\bullet}$ appears as a result of the radical cation decomposition:

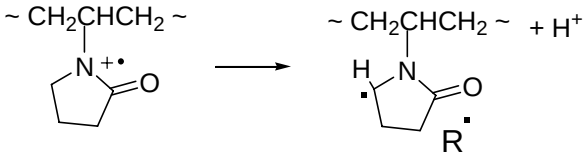

(43)

The decrease of relative yield of radicals R_{im} on addition of polymers with amide groups to composites (figure 3) is apparent from the formal kinetic scheme:

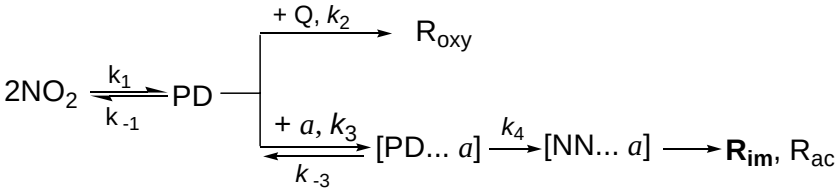

(44)

where *a* is an amide group. Taking into consideration stationary state for concentrations of PD, NN, [PD···*a*], [NN···*a*] and invariance of Q contents in composites, the following equations for rates of accumulation of radicals R_{oxy}, R_{im} and R_{ac} can be obtained:

$$\frac{d[\mathrm{R_{oxy}}]}{dt} = \frac{k_1 k_2 (k_{-3} + k_4)[\mathrm{NO_2}]^2}{(k_{-3} + k_4)(k_{-1} + k_2 + k_3[a]) - k_{-3}k_3[a]} \tag{45}$$

$$\frac{d[\mathrm{R_{im}}],[\mathrm{R_{ac}}]}{dt} = \frac{k_1 k_3 k_4 [a][\mathrm{NO_2}]^2}{(k_{-3} + k_4)(k_{-1} + k_2 + k_3[a]) - k_{-3}k_3[a]}, \tag{46}$$

where $[\mathrm{NO_2}]$ is the concentration of nitrogen dioxide in gas phase, [*a*] is the surface concentration of amide groups. These equations can be simplified if concentrations of amide groups in composites are comparatively high, and the conversion of PD into NN occurs enough effectively, that is $k_3[a] >> k_{-1} + k_2$. Then

$$\frac{d[\mathrm{R_{oxy}}]}{dt} = \frac{k_1 k_2 (k_{-3} + k_4)[\mathrm{NO_2}]^2}{k_3 k_4 [a]} \tag{47}$$

$$\frac{d[\mathrm{R_{in}}],[\mathrm{R_{ac}}]}{dt} = k_1 [\mathrm{NO_2}]^2 \tag{48}$$

Thus the rate of accumulation of radicals R_{im} and R_{ac} is determined by $[\mathrm{NO_2}]$, and concentrations of these radicals accumulated on exposure to nitrogen dioxide do not depend appreciably on AP and PVP contents (figure 3 a, b (curve 2)). In contrast, the yield of R_{oxy} decreases as polyamides are added to composites and [*a*] is increased. These plots in

character are representative of competitive pathways for PD interactions with Q and amide groups. Note that the yield of R_{oxy} is not changed in the NO_2 atmosphere in composites of Q with other polymers, for instance, acetyl cellulose at any ratio of the components.

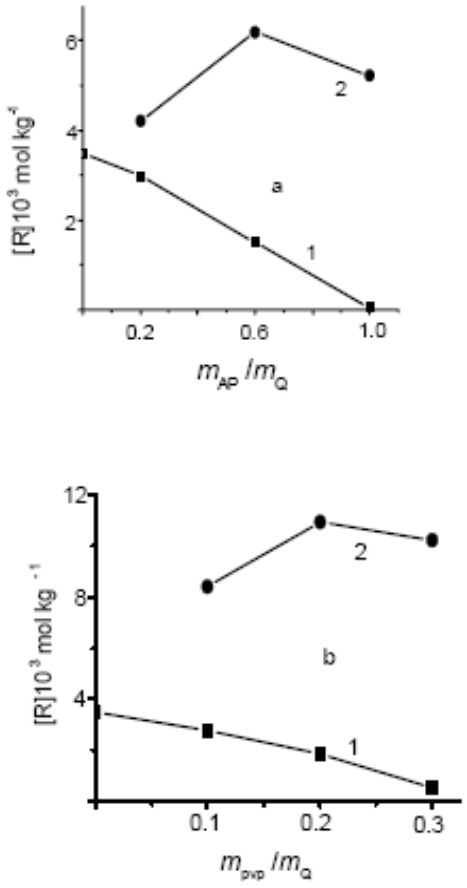

Figure 3. Dependence of concentrations of radicals R_{oxy} (1), R_{im} (2) in Q + AP (a) and R_{oxy} (1), R_{im} + R_{ac} (2) in Q + PVP (b) after exposure to NO_2 on weight ratio of Q, AP and PVP.

VI. Ab Initio Calculations of Energies for Conversions of Nitrogen Dioxide Dimmers

For validating the mechanism proposed of the conversion of PD into NN, the calculations of energy changes in process of nitrogen dioxide interaction with simplest amide (formamide) have been carried out within the framework of density functional theory by the Gaussian 98 program [44]. The B3LYP restricted method for closed and open shells was used. The intention of the calculations is to correlate energy consumptions for PD $\rightarrow$ NN with those for other stages of the radical generation process. Energies of the following states according to scheme (44) were calculated:

$2NO_2 + NH_2COH$ (49)
$O_2N\text{-}NO_2 + NH_2COH$ (50)
$ONONO_2 + NH_2COH$ (51)
$[O_2N\text{-}NO_2 \cdots NH_2COH]$ (52)
$[ONONO_2 \cdots NH_2COH]$ (53)
$N^{\bullet}HCOH + NO + HNO_3$ (54)
$NH_2CO^{\bullet} + NO + HNO_3$ (55)

The geometry optimization of all structures was performed applying the basis set 6-31G (d, p). The given process includes intermediate molecular complexes of PD and NN with formamide (52, 53). The changes of minimum energies are shown in figure 4. One can see that the formation of PD from NO_2 is energetically advantageous process [33], whereas NN is generated from NO_2 in an endothermic reaction. The complexation of PD with formamide is accompanied by release of energy: ΔE = 28 kJ·mol^{-1}. However, PD in complex (52) is not capable of reacting with formamide and can only leave the reacting cage. At the same time, PD in the complex can be converted approximately with the same energy consumption into NN (53), which further reacts by the electron transfer reactions (54, 55) giving radicals, nitric oxide, nitric acid and significant release of energy (44-57 kJ·mol^{-1}). Such sequence of transformations seems to be more efficient in comparison with a direct interaction of NN and formamide by state (51), as the energy of dimers in complexes (52) and (53) is lower than that of initial state (49).

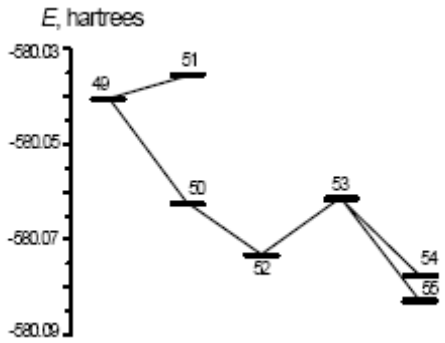

Figure 4. Changes of minimum energies calculated for reactions of NO_2 with formamide.

VII. Detecting Radical Cations in Reactions of Electron Transfer to NN

Registration of radical cations by the EPR method in the presence of nitrogen dioxide could provide direct experimental evidence that the initiation proceeds through scheme (36).

However, because of high reactivity and fast decomposition [45], these particles are difficult to detect by this method. Nevertheless, the formation of radical cations can be revealed indirectly in the act of their decomposition with emission of a proton. Pyridine is known to be capable of accepting protons to yield pyridinium cations. Hence, if protons are

formed in during decomposition of radical cations by reactions (36), they can be detected easily from IR spectra typical of pyridinium cations. Note that pyridine can be nitrated only under quite severe conditions. For example, *N*-nitropyridinium nitrate was obtained only when pyridine was treated with a NO2 –ozone mixture in an inert solvent [46]. This is evident from the IR spectrum (figure 5) of 1:1 mixture of pyridine and *N*-methylpyrrolidone (low-molecular analog of PVP) after treating it by nitrogen dioxide. In the spectrum there are two intense bands at 2400-2600 and 2200 cm^{-1} of pyridinium cations [47]. The scheme of reactions in the given system involves the following consecutive stages:

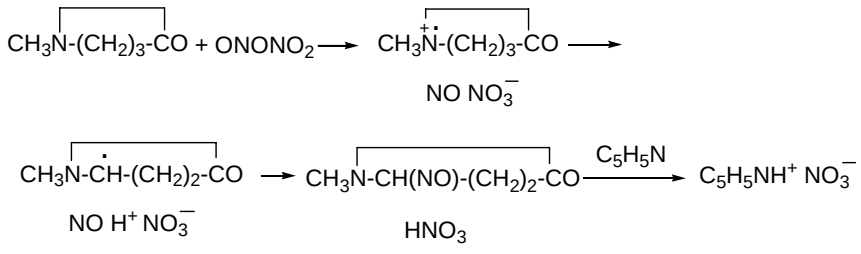

(56)

Thus pyridine fixes occurrence of radical cations as a result of an electron transfer to NN, and in doing so the ion - radical mechanism (36) is experimentally confirmed. It is possible to believe that such oxidative mechanism of generating radicals is characteristic for compounds with the ionization potential providing an electron transfer from donor groups of molecules to NN. This regularity can be followed from examples of thermal and photochemical nitration of aromatic compounds under the action of nitrogen dioxide. According UV spectroscopy data, NN can form charge-transfer complexes with methylbenzenes [48,49]. For the complexes, a bathochromic shift in the corresponding absorption bands was observed with an increase in number of methyl substituents in the benzene ring. Given this, this shift correlates with a decrease in the ionization potential from 8.44 to 7.85 eV on passage from *p*-xylene to hexamethylbenzene.

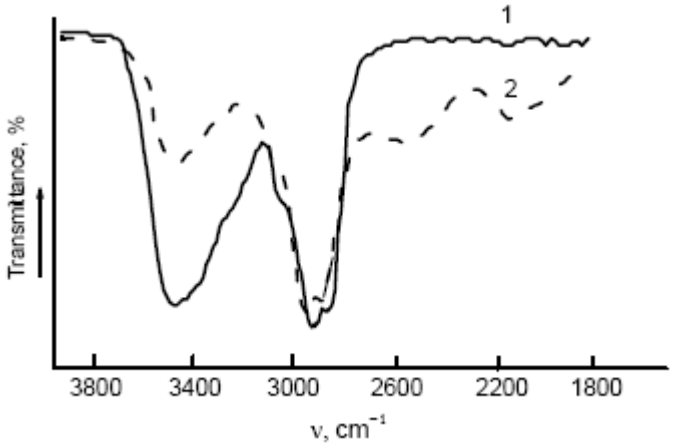

Figure 5. IR spectra of 1:1 *N*-methylpyrrolidone and pyridine mixture (1) and after exposure of the mixture to NO_2 (2).

CONCLUSION

Nitrogen oxides are the effective initiators of radical reactions in a number polymers with formation the various molecular nitration products and stable nitrogen-containing radicals. Nitrogen oxide does not react directly, but it recombines with free radicals formed in polymers by UV photolysis or γ ─ radiolysis. The nitro compounds formed in the subsequent reactions are converted into stable radicals. By this way, spin labels can be inserted even to chemically inert polyperfluoroalkanes. However, the chemical structure of macromolecules can essentially change in enough severe conditions of generating radicals. In this connection, nitrogen trioxide obtained by photolysis of the Ce (IV) nitrates is promising in application for spin labels synthesis. Under the action of visible and near UV light on these additives, the radicals and nitrogen oxide are formed simultaneously with transformation finally into spin labels. The light of such spectral composition does not cause undesirable side effects on macromolecules. Nitrogen dioxide is capable of interacting with least strong C─H and double C=C bonds initiating thus radical reactions in the given system. The dimeric forms of nitrogen dioxide actively react by mechanism depending on the chemical structure of those. The dimers in the form of nitrosyl nitrate represent oxidizing agent initiating ion-radical reactions with formation of stable nitrogen-containing radicals. Amide groups can induce a transition of energetically steadier planar dimers of NO_2 into nitrosyl nitrate. This specific ion-radical mechanism determines high activity relative to NO_2 even such stable polymers as aromatic polyamides.

REFERENCES

[1] R. A. Graham, and H. S. Johnston, *J. Phys. Chem.*, 1978, 82 (3), p. 254.

[2] H. S. Johnston and R. A. Graham, *Canad. J. Chem.*, 1974, 52 (8), p. 1415.

[3] C. Stroud, S. Madronich, E. Atlas, B. Ridley, F. Flocke, A. W. Tallot, A. Fried, B. Wert, R. Shetter, B. Lefler, M. Coffey and B. Heik, *Atmospheric Environment,* 2003, 37 (24), p. 3351.

[4] D. Q. Tong, D. Kang, V. P.Aneja and J. D. Ray, *Ibid.*, 2005, 39 (2), p. 315.

[5] A. I Titov, *Tetrahedron*, 1963, 19, p. 557.

[6] A. V. Topchiev, *Nitration of hydrocarbons and other organic compounds,* Moscow, Academy of Sciences of the USSR, 1956.

[7] S. S. Novikov, G. A. Shveyhgeymer, V. V. Sevastyanova and V. A. Shlyapochnikov, *In Chemistry of aliphatic alicyclic nitro compounds.* 1974, Moscow, Khimiya.

[8] G. B. Pariiskii, I. S. Gaponova and E. Ya. Davydov, *Russ. Chem. Rev.*, 2000, 69 (11), p. 985.

[9] G. B. Pariiskii, I. S. Gaponova, E. Ya Davydov and T. V Pokholok, In *Aging of polymers, polymer blends and polymer composites.* Ed. G. E. Zaikov, A. L. Buchachenko, V. B Ivanov, New York, Nova Science Publishers, 2002.

[10] A. M. Vasserman and A. L. Kovarsky, Spin labels and spin probes in physical chemistry of polymers, Moscow, Nauka, 1986.

[11] I. S. Gaponova, E. Ya. Davydov, G. B. Pariiskii and V. P. Pustoshny, *Vysokomol. Soed.*, ser. A, 2001, 43, (1), p. 98.

[12] T. V. Pokholok, I. S. Gaponova, E. Ya. Davydov and G. B. Pariiskii, *Polym. Degrad. Stability*, 2006, 91 (10), p. 2423.
[13] F. T. Bonner and G. Stedman, *In Methods in nitric oxide research*, Ed. M. Feelish and J. S. Stamler, Chichester, Wiley, 1996.
[14] B. Rånby and J. F. Rabek, *Photodegradation, photo-oxidation and photostabilization of polymers*, London, Wiley, 1975.
[15] J. S. B. Park and J. C. Walton, *J. Chem. Soc., Perkin Trans. 2*, 1997, p. 2579.
[16] I. S. Gaponova, G. B. Pariiskii and D. Ya. Toptygin, *Vysokomolek. Soed.*, 1988, 30 (2), p. 262.
[17] I. S. Gaponova, G. B. Pariiskii and D. Ya. Toptygin, *Khimich. Fizika*, 1997, 16 (10), p. 49.
[18] P. Neta and R. E. Huie, *J. Phys. Chem.*, 1986, 90 (19), p. 4644.
[19] B. Vencatachalapathy and R. Ramamurthy, *J. Photochem. Photobiology A: Chem.*, 1996, 93, p. 1.
[20] S. M. Japar and H. H. Niki, J. *Phys. Chem.*, 1975, 79 (16), p. 1629.
[21] R. Atkinson, C. N. Plum, W. P. L. Carter, A. M. Winer and J. N. Pitts, *J. Phys. Chem.*, 88 (6), p. 1210.
[22] O. Itho, S. Akiho and M. Iino, *J. Org. Chem.*, 1989, 54 (10), p. 2436.
[23] A. K. Pikaev, G. K. Sibirskaya, E. M. Shyrshov, P. Ya Glazunov and V. I. Spicyn, *Dokl. Akad. Nauk SSSR*, 1974, 215 (3), p. 645.
[24] E. Hayon and E. Saito, *J. Chem Phys.*, 1965, 43 (12), p. 4314.
[25] L. Dagliotti and E. Hayon, *J. Phys. Chem.*, 1967, 71 (12), p. 3802.
[26] P. W. Glass and T. W. Martin, *J. Am. Chem. Soc.*, 92 (17), p. 5084.
[27] P. H. Wine, R. L. Mauldin and R. P. Thorn, *J. Phys. Chem.*, 1988, 92 (5), p. 1156.
[28] E. Ya. Davydov, E. N. Afanas'eva, I. S. Gaponova and G. B. Pariiskii, *Org. Biomol. Chem.*, 2004, 2 (9), p. 1339.
[29] E. Ya. Davydov, I. S. Gaponova and Pariiskii, *Vysokomolek. Soed.*, ser. A, 2003, 45, (4), p. 581.
[30] H. J. Naghash, A. Massah and A. Erfan, *Eur. Polym. J.*, 2002, 38, (1), p. 147.
[31] H. H. G. Jellinek, *Aspects of degradation and stabilization of polymers. Chapter 9.* New York, Elsevier, 1978.
[32] D. H. Giamalva, G. B. Kenion and W. A. Pryor, *J. Am. Chem. Soc.*, 1987, v. 109. № 23, p. 7059.
[33] P. Golding, J. L. Powell and J. H. Ridd, *J. Chem. Soc., Perkin Trans. 2*, 1996, p. 813.
[34] M. Gyor, A. Rockenbauer and F. Tüdos, *Tetrahedron Lett.*, 1986, 27 (39), p. 4795.
[35] T. V. Pokholok and G. B. Pariiskii, *Vysokomolek. Soed., ser. A*, 1977, 39 (7), p. 1152.
[36] A. I. Smirnov, E. N. Degtyarev, O. E. Yakimchenko and Ya. S. Lebedev, *Pribory Tekhn. Eksperim*, 1991, 1,p. 195.
[37] E. N. Degtyarev, T. V. Polholok, G. B. Pariiskii O. E. Yakimchenko, *Zh. Fiz. Khim.*, 1994, 68 (3), p. 461.
[38] M. L. McKee, *J. Am. Chem. Soc.*, 1995, 117 (8), p. 1629.
[39] E. H. White, *Ibid.*, 1955, 77, (20), p. 6008.
[40] E. Ya. Davydov, I. S. Gaponova, G. B. Pariiskii and T. V. Pokholok, *Polm. Sci., ser.A*, 2006, 48 (4), p. 375.
[41] H. Feuer, *The chemistry of the nitro and nitroso groups*, New York, Wiley, 1969.

[42] E. Ya. Davydov, I. S. Gaponova and G. B. Pariiskii, *J. Chem. Soc., Perkin Trans. 2,* 2002, p. 1359.
[43] I. Gabr and M. C. R. Symons, *J. Chem. Soc., Faraday Trans*., 1996, 92 (10), p. 1767.
[44] M. J. Frisch, G. W. Trucks, H. B. Schlegel, G. E. Scuseria, M. A. Robb, J. R. Cheeseman et al.: Gaussian 98. Pitsburgh, PA, Gaussian Inc., 1998.
[45] D. Greatorex and J. Kemp, *J. Chem. Soc., Faraday Trans*., 1972, 68 (1), p. 121.
[46] H. Suzuki, M. Iwaya and T. Mori, *Tetrahedron Lett*., 1997, 38 (32), p. 5647.
[47] L. J. Bellamy, *The infra-red spectra of complex molecules.* London, Methuen, 1957.
[48] E. Bosch and J. K. Kochi, *J. Org. Chem.*, 1994, 59 (12), p. 3314.
[49] T. M. Bockman, Z. J. Karpinski, S. Sankararaman and J. K. Kochi, *J. Am. Chem. Soc*., 1992, 114, (6), p. 1970.

In: Monomers, Oligomers, Polymers, Composites… ISBN: 978-1-60456-877-6
Editors: R. A. Pethrick, G.E. Zaikov et al.

Chapter 5

A NOVEL TECHNIQUE FOR MEASUREMENT OF ELECTROSPUN NANOFIBER

M. Ziabari, V. Mottaghitalab and A. K. Haghi*
University of Guilan, P. O. Box 3756, Rasht, Iran

ABSTRACT

In electrospinning, fiber diameter is an important structural characteristic because it directly affects the properties of the produced webs. In this chapter, we have developed an image analysis based method called direct tracking for measuring electrospun fiber diameter. In order to evaluate its accuracy, samples with known characteristics have been generated using a simulation scheme known as μ-randomness. To verify the applicability of the method, some real webs obtained from electrospinning of PVA have been used. Due to the need of binary input images, micrographs of the real webs obtained from scanning electron microscopy were segmented using local thresholding. The method was compared with the distance transform method. Results obtained by direct tracking were significantly better than distance transform, indicating that the method could be used successfully for measuring electrospun fiber diameter.

Keywords: Electrospinning, Fiber diameter, Image analysis, Direct tracking, Distance transform

1. INTRODUCTION

Conventional fiber spinning (like melt, dry and wet spinning) produce fibers with diameter in the range of micrometer. In recent years, electrospinning has gained much attention as a useful method to prepare fibers in nanometer diameter range. These ultra-fine fibers are classified as nanofibers. The unique combination of high specific surface area, extremely small pore size, flexibility ad superior directional strength makes nanofibers a

* Haghi@Guilan.ac.ir

preferred material form for many applications. Proposed uses of nanofibers include wound dressing, drug delivery, tissue scaffolds, protective clothing, filtration, reinforcement and micro-electronics.

In the electrospinning process, a polymer solution held by its surface tension at the end of a capillary tube is subjected to an electric field. Charge is induced on the liquid surface by an electric field. Mutual charge repulsion causes a force directly opposite to the surface tension. As the intensity of the electric field is increased, the hemispherical surface of the solution at the tip of the capillary tube elongates to form a conical shape known as the Taylor cone. When the electric field reaches a critical value at which the repulsive electric force overcomes the surface tension force, a charged jet of the solution is ejected from the tip of the cone. Since this jet is charged, its trajectory can be controlled by an electric field. As the jet travels in air, the solvent evaporates, leaving behind a charged polymer fiber which lays itself randomly on a collecting metal screen. Thus, continuous fibers are laid to form a nonwoven fabric. Figure 1 illustrates the electrospinning setup [1-[6].

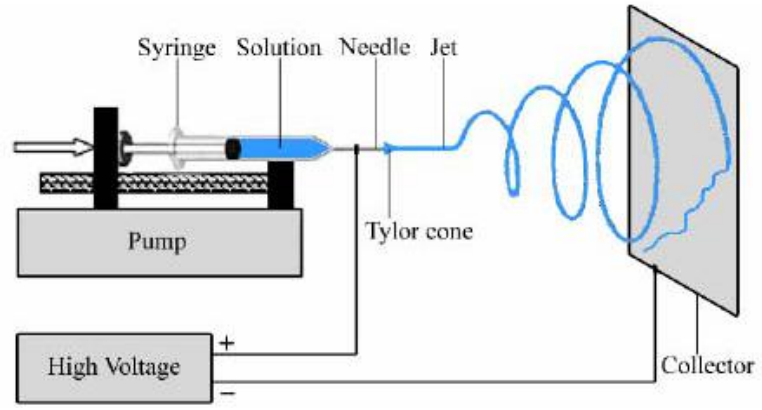

Figure 1. Electrospinning setup.

The properties of electrospun nonwoven webs depend on the nature of the component fiber as well as its structural characteristics such as fiber orientation [7]-[12] fiber diameter[13], pore size [15], uniformity and other structural features [16]. Analyzing the electrospun webs yield results and information, which will help researchers in improving the quality and predicting the overall performance of the electrospun webs. Some of the reasons for characterization may be process control, process development and product or quality control. Fiber diameter is the most important structural characteristics in electrospun nonwoven webs. Depending on the process and material variables the diameter of the fibers produced by electrospinning varies. Almost all researches who have done characterization, have reported the effects of processing variables on electrospun fiber diameter. There is no standard technique to measure the fiber diameter and analyze its distribution. This explains the need to study the fiber diameter of electrospun webs. Recently, image analysis has been used to identify fibers and measure structural characteristics in nonwovens. However, the accuracy and the limitations of these techniques have not been verified.

The objective of our research is to use image analysis for measuring electrospun fiber diameter.

2. METHODOLOGY

2.1. Simulation of Electrospun Web

In order to reliably evaluate the accuracy of the developed methods, samples with known characteristics are required. Since this end cannot be met with experiment, a simulation algorithm has been employed for generating nonwovens with known characteristics. The use of simulation is not a new idea. It was used by Abdel-Ghani and Davis [17]] and Pourdeyhimi et. al. [7] for simulation of nonwovens with both continuous and discontinuous fibers by the use of idealized straight lines. The most important component of simulation is the way in which lines or curves are generated. Abdel-Ghani and Davis [17] presented three methods for generating a random network of lines.

1. Surface randomness known as S-randomness
2. Mean free path known as μ-randomness
3. Internal randomness known as I-randomness

It is assumed that the lines are infinitely long (continuous filament) so that, at least in the image plane, all lines intersect the boundaries.

The aim is to obtain unbiased arrays which are spatially homogeneous for infinitely long lines. Lately it was discovered by Pourdeyhimi et. al. [7] that the best way to simulate nonwovens of continuous fibers is through the second method. Under this scheme, a line with a specified thickness is defined by the perpendicular distance d from a fixed reference point O located in the center of the image and the angular position of the perpendicular α. Distance d is limited to the diagonal of the image [7], [17]. Figure 2 demonstrates this procedure.

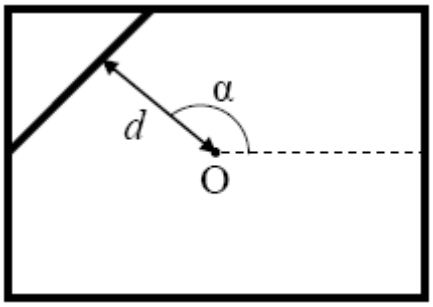

Figure 2. Procedure for μ-randomness.

Seeveral variables are allowed to be controlled during the simulation.

1. Web density: can be controlled using the line density which is the number of lines to be generated in the image.
2. Angular density: useful for generating fibrous structures with specific orientation distribution. The orientation may be sampled from either a normal or a uniform random distribution.

3. Distance from the reference point: varies between 0 and the diagonal of the image, restricted by the boundary of the image and is sampled from a uniform random distribution.
4. Line thickness (fiber diameter): is sampled from a normal distribution. The mean diameter and its standard deviation are needed.
5. Image size: can also be chosen as required.

2.2. Fiber Diameter Measurement

Electrospinning process produces very fine fibers and this is one of the few methods from which fibers of sub-micron size can be produced. So it becomes immensely important to understand the behavior of fiber diameter and fiber diameter distribution in the electrospun web as impacted by the processing parameters. The first step in determining fiber diameter is to produce a high quality image of the web at a suitable magnification using electron microscopy techniques, called micrograph. The methods for measuring electrospun fiber diameter are described in following sections.

2.2.1. Manual Method

The conventional method of measuring the fiber diameter of electrospun webs is to analyze the micrograph manually. The manual analysis usually consists of the following steps, determining the length of a pixel of the image (setting the scale), identifying the edges of the fibers in the image and counting the number of pixels between two edges of the fiber (the measurements are made perpendicular to the direction of fiber-axis), converting the number of pixels to nm using the scale and recording the result. Typically 100 measurements are carried out. Figure 3 illustrates this process.

However, this process is tedious and time-consuming especially for large number of samples. Furthermore, it cannot be used as on-line method for quality control since an operator is needed for performing the measurements. Thus, developing automated techniques which eliminate the use of operator and has the capability of being employed as on-line quality control is of great importance.

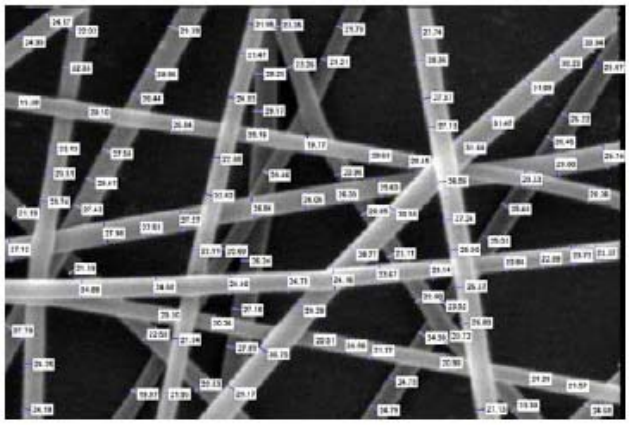

Figure 3. Manual method.

2.2.2. Distance Transform

The distance transform of a binary image is the distance from every pixel to the nearest nonzero-valued pixel. The center of an object in the distance transform image will have the highest value and lie exactly over the object's skeleton. The skeleton of the object can be obtained by the process of skeletonization or thinning. The algorithm removes pixels on the boundaries of objects but does not allow objects to break apart. This reduces a thick object to its corresponding object with one pixel width. Skeletonization or thinning often produces short spurs which can be cleaned up automatically with a pruning procedure [18].

The algorithm for determining fiber diameter uses a binary input image and creates its skeleton and distance transformed image. The skeleton acts as a guide for tracking the distance transformed image by recording the intensities to compute the diameter at all points along the skeleton. This method was proposed by Pourdeyhimi et. al. [13]. Figure 4 shows a simple simulated image, its skeleton overlaid on its distance transform and the histogram of fiber diameter obtained by this method.

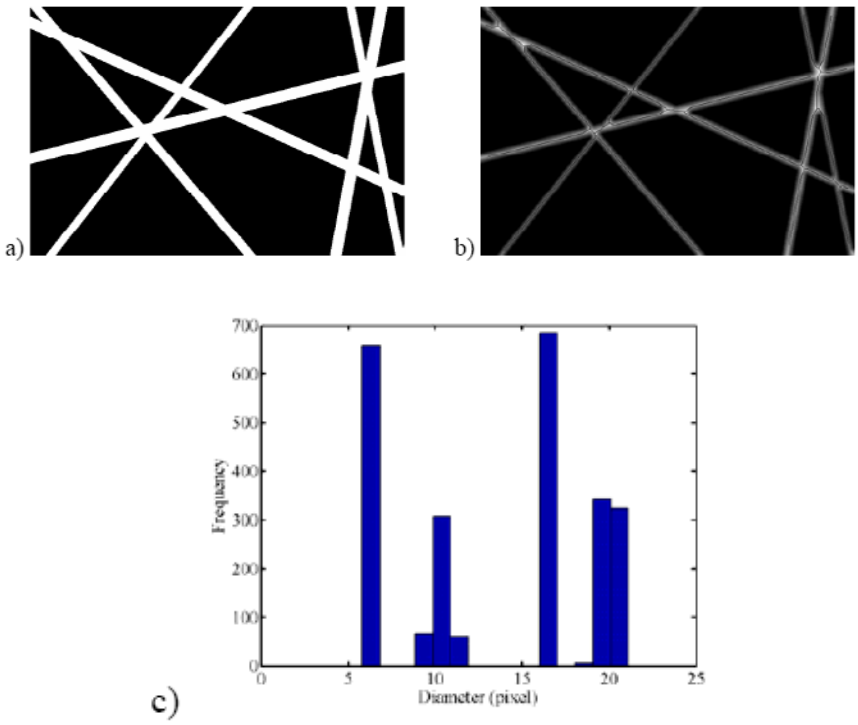

Figure 4. a) A simple simulated image, b) Its skeleton overlaid on its distance transform, c) Histogram of fiber diameter distribution obtained by distance transform.

2.2.3. Direct Tracking

In order to measure the electrospun fiber diameter, we developed an image analysis based method called Direct Tracking. This method in which a binary image is used as an input determines fiber diameter on the basis of two scans; first a horizontal and then a vertical scan. In the first scan, the algorithm searches for the first white pixel adjacent to a black. Pixels are

counted until reaching the first black. The second scan is then started from the mid point of horizontal scan and pixels are counted until the first black is encountered. If the black pixel isn't found, the direction changes. Having the number of horizontal and vertical scans, the number of pixels in perpendicular direction which is the fiber diameter could be measured from a geometrical relationship. The process is illustrated in Figure 5.

In electrospun webs, fibers cross each other at intersection points and this brings about some untrue measurements in these areas. To circumvent this problem, black regions are labeled and it is identified which couple of regions consist of fiber. Then, in order to enhance the processing speed, the image is cropped to the size of selected regions. Afterwards, fiber diameter is measured according to the explained algorithm. Finally, the data in pixels are converted to nm and the histogram of fiber diameter distribution is plotted. Figure 6 shows a labeled simple simulated image and the histogram of fiber diameter obtained by this method.

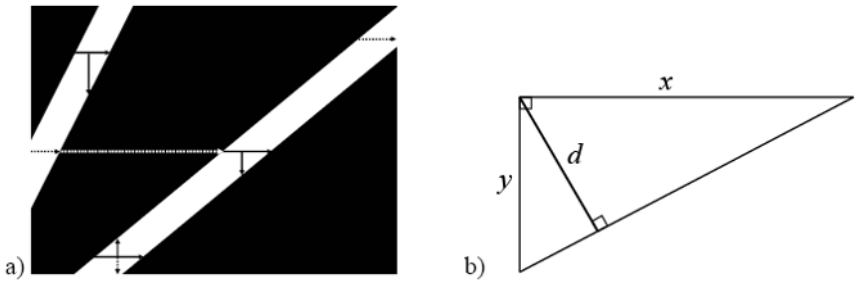

Figure 5. a) Direct tracking, b) Fiber diameter from the number of vertical and horizontal pixels.

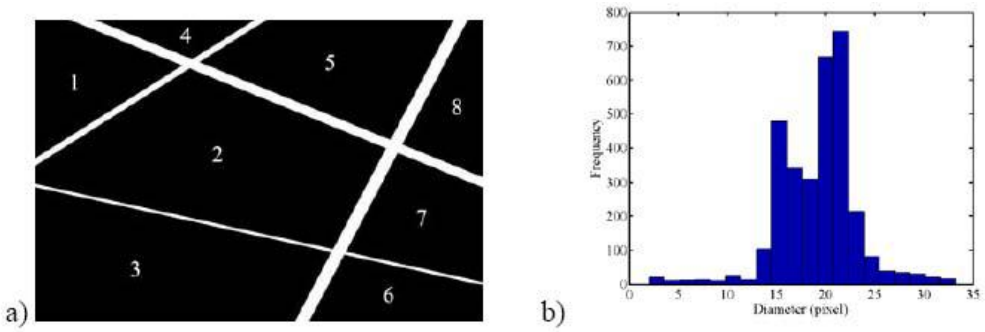

Figure 6. a) A simple simulated image which is labeled, b) Histogram of fiber diameter distribution obtained by direct tracking.

2.3. Real Webs Treatment

Both of distance transform and direct tracking algorithm for measuring fiber diameter require binary image as input. Hence, the micrographs first have to be converted to black and white. This is done by thresholding (known also as segmentation) which produces binary image from a grayscale (intensity) image. This is critical step because the segmentation affects the result. In the simplest thresholding technique, called global thresholding, the image is partitioned using a single constant threshold. One simple way to choose a threshold is by

trial and error. Then each pixel is labeled as object or background depending on whether the gray level of that pixel is greater or less than the value of threshold respectively.

The main problem here is global thresholding can fail in the presence of non-uniform illumination or local gray level unevenness. An alternative to circumvent this problem is to use local thresholding instead. In this approach, the original image is divided to subimages and different thresholds are used for segmentation. Another variation of this approach which has been used in this study consists of estimating the background illumination using morphological opening operation, subtracting the obtained background from the original image and applying a global thresholding to produce the binary version of the image. In order to automatically compute the appropriate threshold, Ostu's method could be employed. This method chooses the threshold to minimize interaclass variance of the black and white pixels. Prior to the segmentation, an intensity adjustment operation and a two dimensional median filter were applied in order to enhance the contrast of the image and remove noise [8]-[21]. As it is shown in Figure 7, global thresholding resulted in some broken fiber segments. This problem was solved using local thresholding.

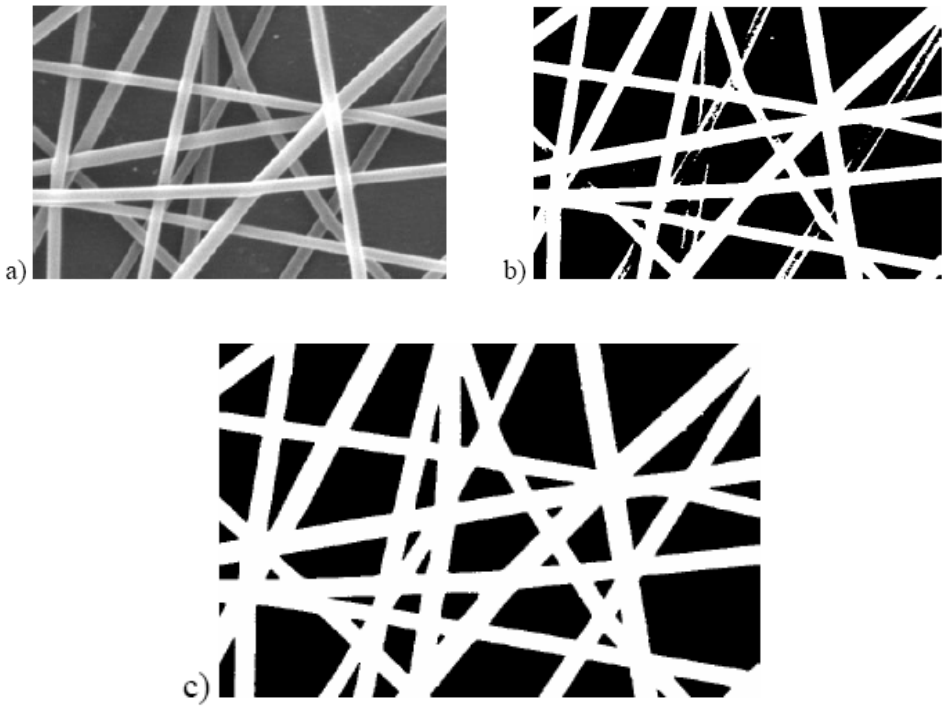

Figure 7. a) A real web, b) Global thresholding, c) Local thresholding.

3. EXPERIMENTAL

Electrospun nonwoven webs used as real webs in image analysis obtained from electrospinning of PVA with average molecular weight of 72000g/mol, purchased from MERCK Company, at different processing parameters. The micrographs of the webs were obtained using Philips (XL-30) environmental Scanning Electron Microscope (SEM) under

magnification of 10000X after being gold coated. Figure 8 shows the micrographs of the electrospun webs used as real webs.

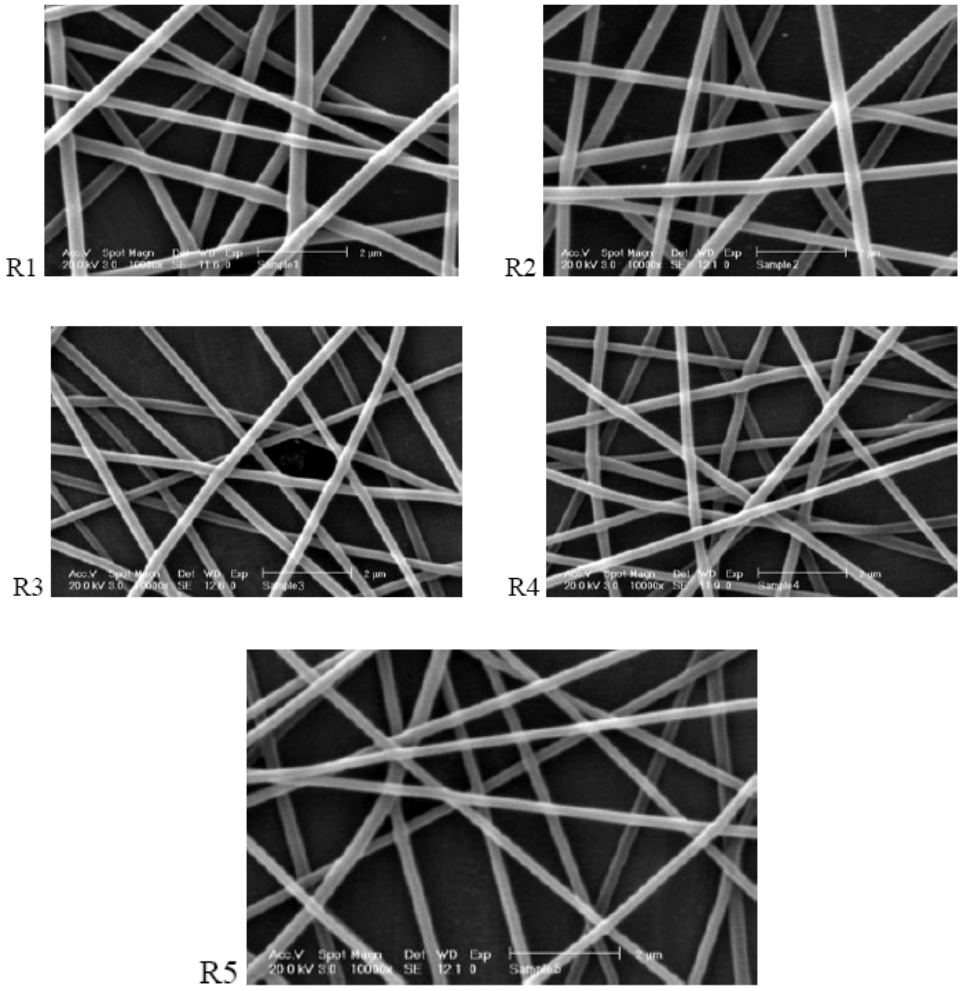

Figure 8. Micrographs of the electrospun webs.

4. RESULTS AND DISCUSSION

Two sets each composed of five simulated images generated by μ-randomness procedure were used as samples with known characteristics to demonstrate the validity of the techniques. The first set had random orientation with increasing constant diameters; the second was also randomly oriented but with varying diameter sampled from normal distributions with a mean of 15 pixels and standard deviations ranging from 2 to 10 pixels. Table 1 and Table 2 show the structural features of these simulated images which are shown in Figure 9 and Figure 10. Moreover, the applicability of the techniques was tested using five real webs obtained from electrospinning of PVA.

Table 1. Structural characteristics of first set images

Image No.	Angular Range	Line Density	Line Thickness
C1	0-360	30	5
C2	0-360	30	10
C3	0-360	30	15
C4	0-360	30	20
C5	0-360	30	25

Table 2. Structural characteristics of second set images

Image No.	Angular Range	Line Density	Line Thickness	
			Mean	Std
V1	0-360	30	15	2
V2	0-360	30	15	4
V3	0-360	30	15	6
V4	0-360	30	15	8
V5	0-360	30	15	10

Mean and standard deviation of the simulated images in the first and second set are shown in Table 3 and Table 4 respectively. Table 5 shows the results for real webs in term of pixel and nm. show histograms of fiber diameter distribution for simulated images in the first and second set respectively. Histograms for real webs are given in figure 13..

In the first set, for simulated images with the line thickness of 5 and 10 pixels, distance transform presents mean and standard deviation of fiber diameter closer to the simulation. For the line thickness of 15, the standard deviation of diameter obtained from direct tracking method is closer to that of the simulation. However, in this case distance transform measured the average diameter more accurately. For the simulated webs with line thickness more than 15 in the first set, direct tracking method resulted in better estimation of the mean and standard deviation of fiber diameter. This is due to the fact that as the lines get thicker, there is higher possibility of branching during the skeletonization (or thinning) and these branches remain even after pruning. Although these branches are small, their orientation is typically normal to the fiber axis; thus causing widening the distribution.

Table 3. Mean and standard deviation for series 1

		C1	C2	C3	C4	C5
Simulation	mean	5	10	15	20	25
	std	0	0	0	0	0
Distance Transform	mean	5.486	10.450	16.573	23.016	30.063
	std	1.089	2.300	5.137	6.913	10.205
Direct Tracking	mean	5.625	11.313	17.589	22.864	29.469
	std	1.113	2.370	4.492	5.655	7.241

Table 4. Mean and standard deviation for series 2

		V1	V2	V3	V4	V5
Simulation	mean	15.247	15.350	15.243	15.367	16.628
	std	1.998	4.466	5.766	8.129	9.799
Distance Transform	mean	16.517	16.593	17.135	17.865	19.394
	std	5.350	6.165	7.597	9.553	11.961
Direct Tracking	mean	16.075	15.803	16.252	16.770	18.756
	std	2.606	5.007	6.129	9.319	10.251

Table 5. Mean and standard deviation for real webs

			R1	R2	R3	R4	R5
Manual	mean	pixel	24.358	24.633	18.583	18.827	17.437
		nm	318.67	322.27	243.11	246.31	228.12
	std	pixel	3.193	3.179	2.163	1.984	2.230
		nm	41.77	41.59	28.30	25.96	29.18
Distance Transform	mean	pixel	27.250	27.870	20.028	23.079	20.345
		nm	356.49	364.61	262.01	301.94	266.17
	std	pixel	8.125	7.462	4.906	7.005	6.207
		nm	106.30	97.62	64.18	91.64	81.21
Direct Tracking	mean	pixel	27.195	27.606	20.638	21.913	20.145
		nm	355.78	361.15	269.99	286.68	263.55
	std	pixel	4.123	5.409	4.148	4.214	3.800
		nm	53.94	70.77	54.27	55.14	49.72

Furthermore, distance transform method fails in measuring the diameter of fiber in intersections. The intersections cause to overestimate fiber diameter. Since in direct tracking method, image is divided into parts where single fibers exist, the effect of intersections which causes in inaccurate measurement of fiber diameter is eliminated. Therefore, there will be a better estimate of fiber diameter.

In the second set, independent of the line thickness in the simulation, for all simulated webs, direct tracking resulted in better measurement of mean and standard deviation of fiber diameter. For the real webs, mean and standard deviation of fiber diameter for direct tracking were closer to those of manual method which concurs with the trends observed for the simulated images. Figure 10. Moreover, the applicability of the techniques was tested using five real webs obtained from electrospinning of PVA.

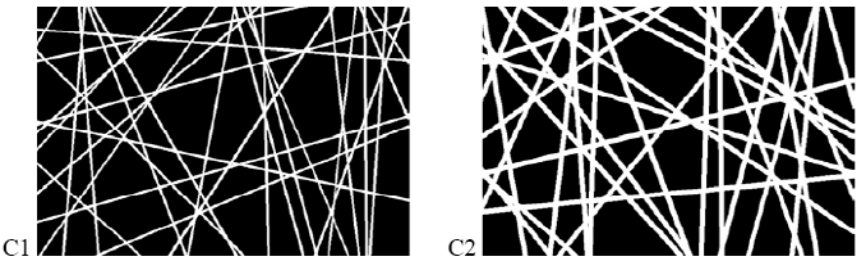

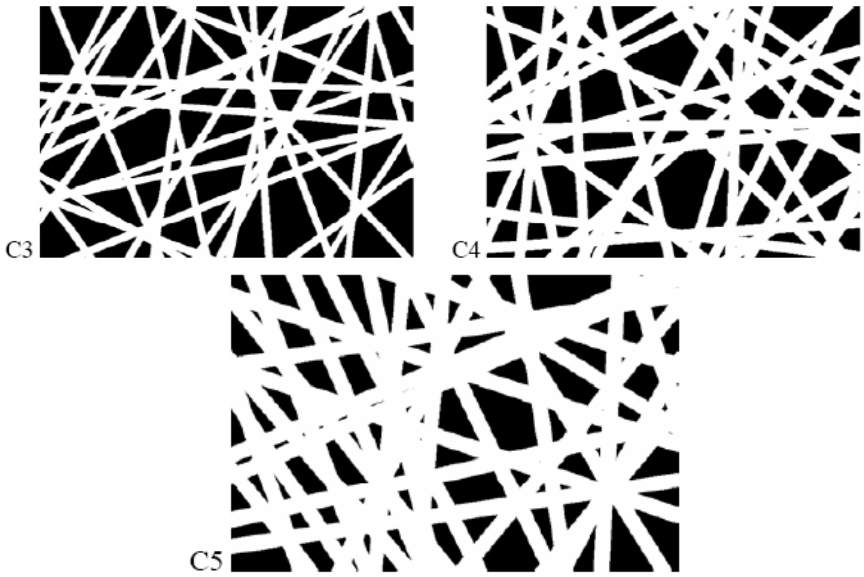

Figure 9. Simulated images with constant diameter.

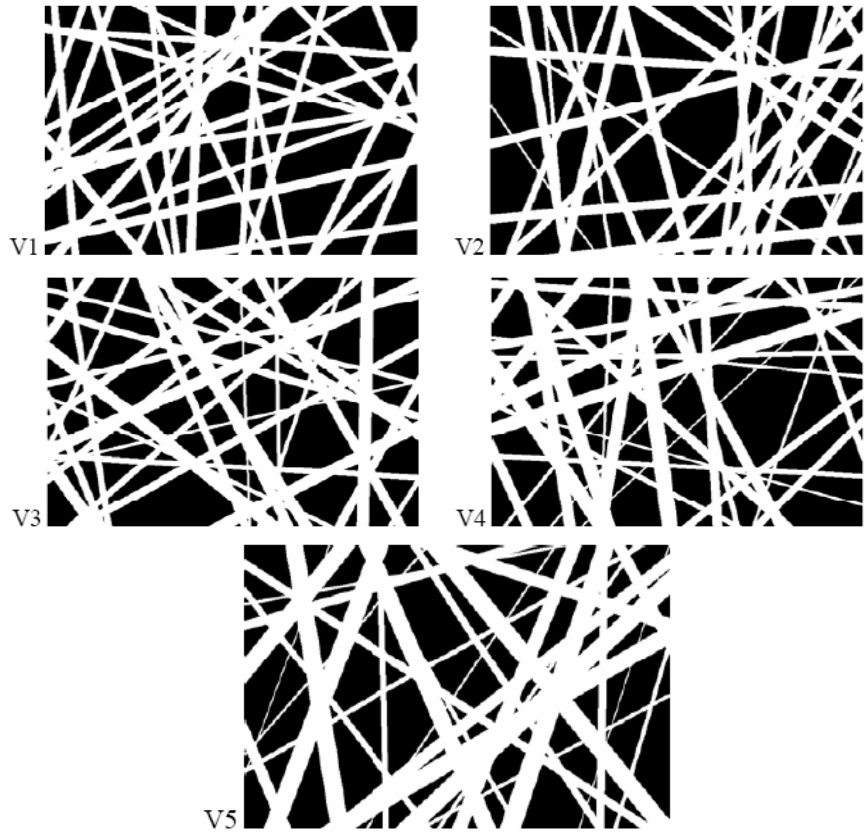

Figure 10. Simulated images with varying diameter.

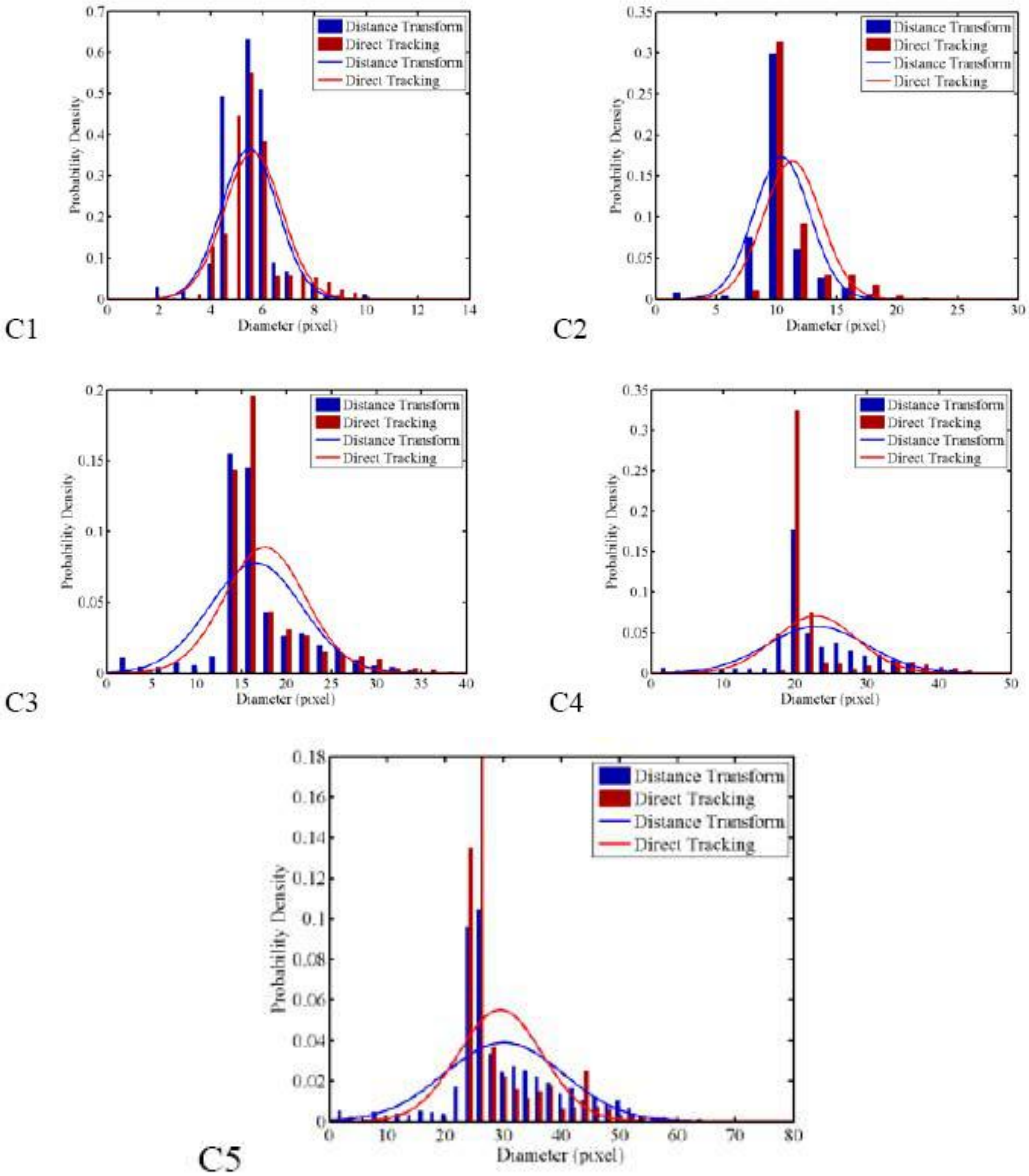

Figure 11. Histograms for simulated images with constant diameter.

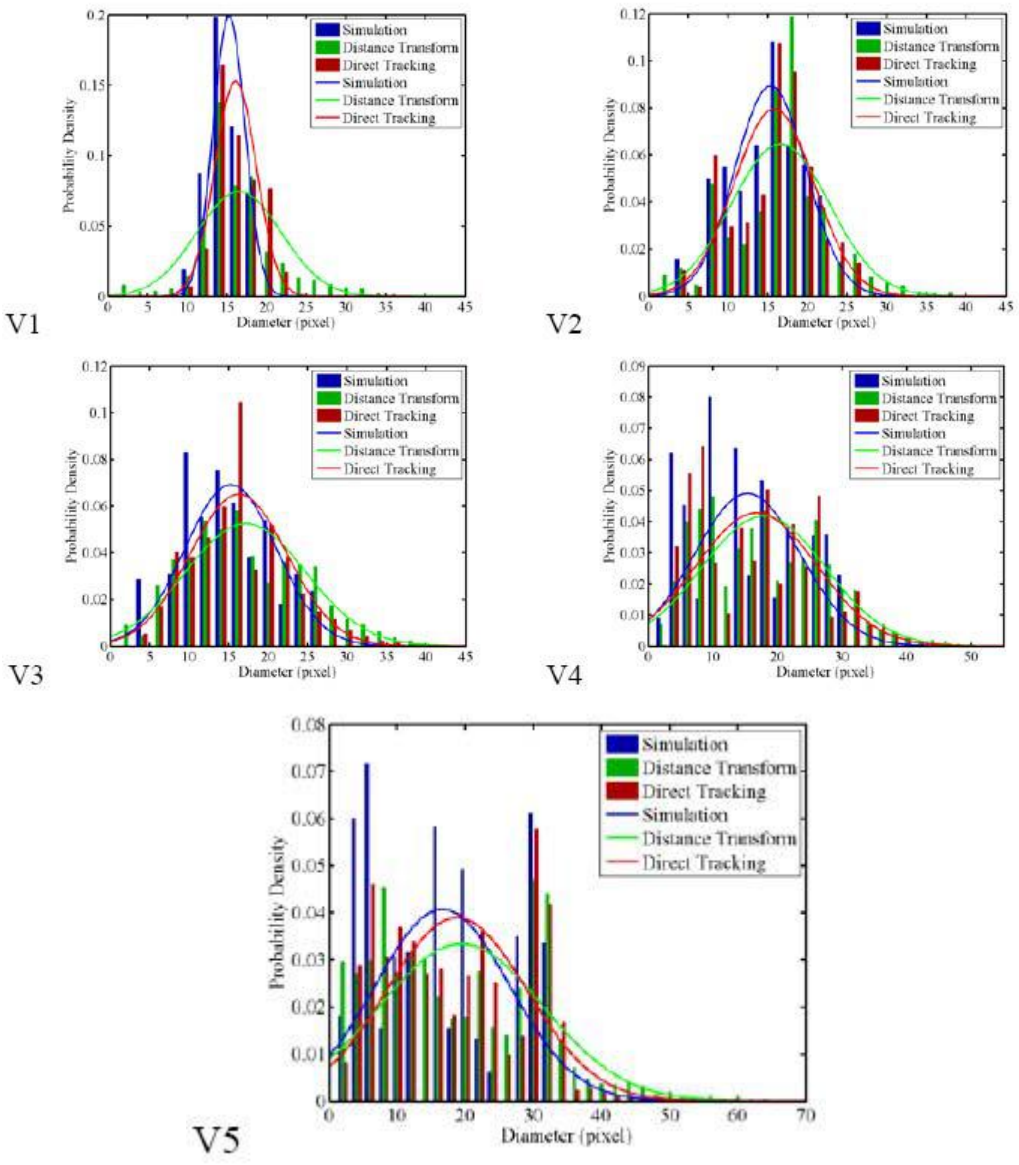

Figure 12. Histograms for simulated images with varying diameter.

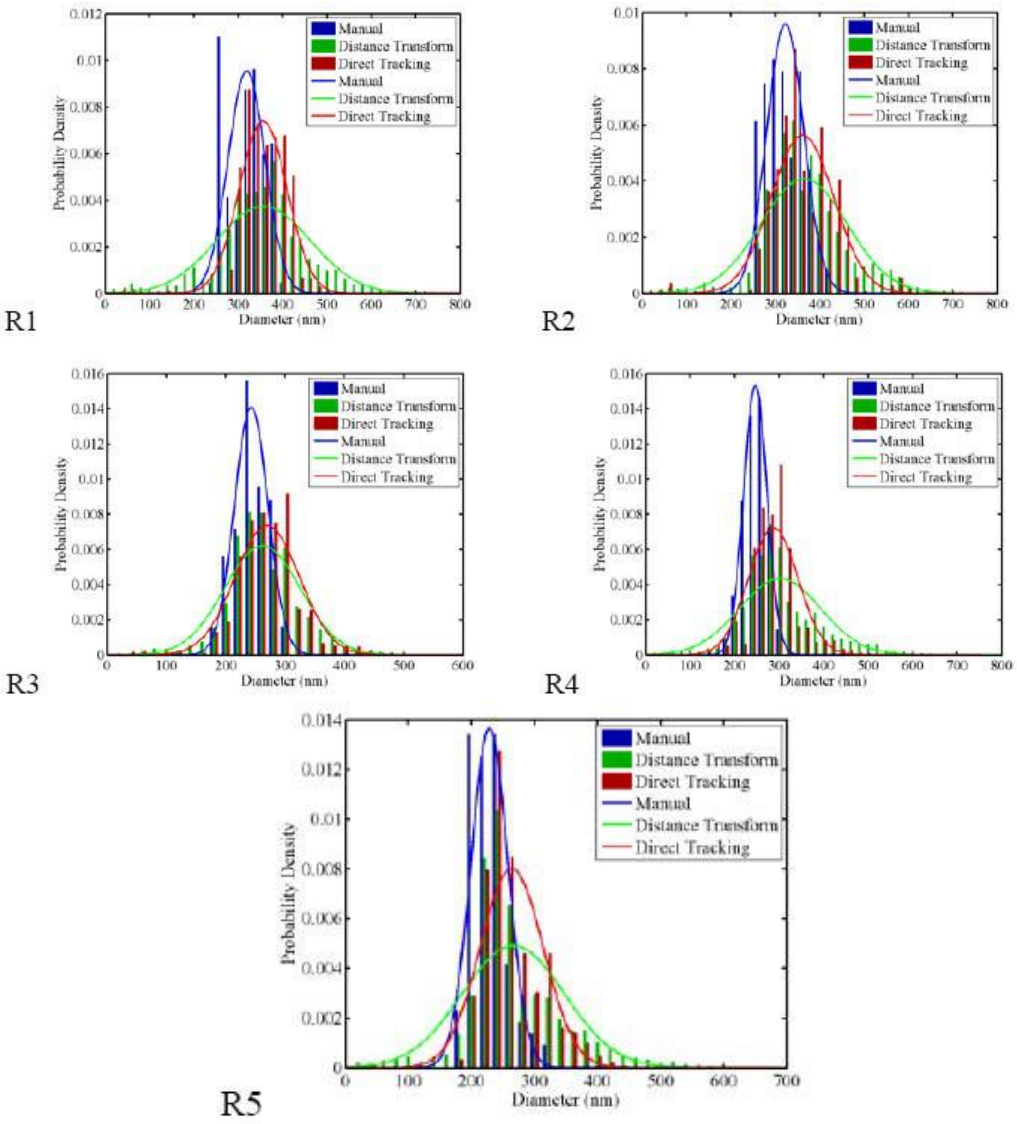

Figure 13. Histograms for real webs.

5. CONCLUSION

Fiber diameter is the most important structural characteristics in electrospun nonwoven webs. The typical way of measuring electrospun fiber diameter is through manual method which is a tedious, time consuming and an operator-based method and cannot be used as an automated technique for quality control. We investigated the use of image analysis for determining fiber diameter and developed an automated method called direct tracking. Since

this is a new technique its accuracy needs to be evaluated using samples with known characteristics. To that end, μ-randomness procedure was used in order to simulate the electrospun nonwoven webs. Based on this scheme, two sets of simulated images, each containing 5 webs, were generated. The first set had random orientation with increasing constant diameter. For the second set, the diameter values were sampled from normal distributions with a mean of 15 and standard deviation ranging from 2 to 10 pixels. We compared our method with the distance transform method. For all the simulated webs with varying diameter and for those with constant diameter more than 15, direct tracking method resulted in the mean and standard deviation closer to the simulation. However, for the simulated webs with smaller constant diameter, distance transform measured the mean and standard deviation of fiber diameter more accurately. The results suggest that the direct tracking method is an accurate, direct measurement technique, because it extracts the fiber diameter for the samples by tracking fixed segment of the fiber and eliminates the effect of intersections.

We have demonstrated the general applicability of the method using real webs. 5 real electrospun nonwoven webs obtained by electrospinning of PVA were used. Since the methods needed binary images as input, the images first had to be segmented. A local thresholding method together with Ostu's method was employed in order to automatically compute the appropriate threshold. The results obtained for real webs confirm the trends suggested by simulated images. The results show that the use of image analysis in order to determine the fiber diameter in electrospun nonwoven webs has been successful.

REFERENCES

[1] A. K. Haghi, M. Akbari, *Physica Status Solidi.* (a) 204 (2007) 1830-1834.

[2] J. Doshi, D. H. Reneker, *Journal of Electrostatics.* 35 (1995) 151-160.

[3] D. H. Reneker, I. Chun, *Nonotechnology.* 7 (1996) 216-223.

[4] H. Fong, D. H. Reneker, Electrospinning and the Formation of Nanofibers, In: D. R. Salem, Structure Formation in polymeric Fibers, Hanser, Cincinnati, 2001, pp. 225-246.

[5] Th. Subbiah, G. S. Bhat, R. W. Tock, S. Parameswaran, S. S. Ramkumar, *Journal of Applied Polymer Science*. 96 (2005) 557-569.

[6] W. Zhang, Z. Huang, E. Yan, Ch. Wang, Y. Xin, Q. Zhao, Y. Tong, *Materials Science and Engineering.* A 443 (2007) 292–295.

[7] B. Pourdeyhimi, R. Ramanathan, R. Dent, *Textile Research Journal.* 66 (1996) 713-722.

[8] B. Pourdeyhimi, R. Ramanathan, R. Dent, *Textile Research Journal.* 66 (1996) 747-753.

[9] B. Pourdeyhimi, R. Dent, H. Davis, *Textile Research Journal.* 67 (1997) 143-151.

[10] B. Pourdeyhimi, R. Dent, *Textile Research Journal.* 67 (1997) 181-190.

[11] B. Pourdeyhimi, R. Dent, A. Jerbi, S. Tanaka, A. Deshpande, *Textile Research Journal.* 69 (1999) 185-92.

[12] B. Pourdeyhimi, H.S. Kim, *Textile Research Journal.* 72 (2002) 803-809.

[13] B. Pourdeyhimi, R. Dent, *Textile Research Journal.* 69 (1999) 233-236.

[14] B. Xu, Y. L. Ting, *Textile Research Journal.* 65 (1995) 41-48.
[15] A. H. Aydilek, S. H. Oguz, T. B. Edil, *Journal of Computing in Civil engineering.* (2002) 280-290.
[16] R. Chhabra, International Nonwoven Journal. (2003) 43-50.
[17] M. S. Abdel-Ghani, G. A. Davis, *Chemical Engineering Science.* 40 (1985) 117-129.
[18] R. C. Gonzalez, R. E. Woods, *Digital Image Processing,* 2nd Edition, Prentice Hall, 2001.
[19] B. Jähne, Digital Image Processing, 5th Revised and Extended Edition, Springer, 2002.
[20] M. Petrou, P. Bosdogianni, Image Processing the Fundamentals, John Wiley and Sons, 1999.
[21] J. Serra, Image Analysis and Mathematical Morphology, Academic Press, London, 1982.

In: Monomers, Oligomers, Polymers, Composites… ISBN: 978-1-60456-877-6
Editors: R. A. Pethrick, G.E. Zaikov et al.

Chapter 6

A STUDY ON THE EFFECTS OF RECYCLED GLASS, SILICA FUME AND RICE HUSK ASH ON THE INTERFACIAL AND MECHANICAL PROPERTIES OF CEMENTITIOUS COMPOSITE

A. Sadrmomtazi and A.K. Haghi*
University of Guilan, P. O. Box 3756, Rasht, Iran

ABSTRACT

The carpet waste fibers as well as waste glass generated each year create a serious environmental problem and accumulated in the landfills which can be converted into useful products. The use of these waste materials in a cement-based composite can be a promising direction for waste reduction and resources conservation. In this study, several tests carried out to investigate the performance of ordinary Portland cement using recycled glass and fibers as a fraction of aggregates used in a cement-based composite. These tests included compressive strength, flexural strength, flexural toughness and water absorption. The results of this study revealed that carpet waste fiber and waste glass could be reused as substitutes for conventional materials in cement-based composites.

1. INTRODUCTION

As the world population grows, so do the amount and type of waste being generated. Many of the wastes produced today will remain in the environment for years to come. The creation of nondecaying waste materials, combined with a growing consumer population, has resulted in a waste disposal crisis. So one of the solutions to improve the environment is recycle and reuse these waste materials in construction.

A great amount of fibrous textile waste is discarded into landfills each year all over the world. More than half of this waste is from carpets, with the main constituents being plastic

* Corresponding author: e-mail: Haghi@Guilan.ac.ir

and polymeric fiber, which decays at a very slow rate and which is difficult to handle in landfills. The development of low-cost technologies to convert textile waste into useful products could reduce disposal pressures on landfills and result in cost savings for carpet industries. Accordingly, many carpet and textile manufacturers, fiber and chemical suppliers, recycling companies, and academic institutions are actively pursuing various methods to recycle and convert fibrous waste into various useful products [ ].

One promising reuse of these wastes lies in concrete reinforcement and construction applications. Extensive studies have been reported in the literature that indicate the use of natural and synthetic fibers in concrete can enhance the tensile strength and flexural toughness characteristics of concrete,

Waste carpet fibers have been used in cement-based composites concrete since the late 1960s [1]. Natural and other synthetic fibers are added to cement as secondary reinforcement to control plastic shrinkage [2]. The effect of polypropylene fibers on the properties of cement-based composites varies depending on the type, length, and volume fraction of fiber, the mixture design, and the nature of materials used.

Although many researchers studied the reuses of polypropylene fibers in cement-based composite but admixture of waste glass in fiber-reinforced cement-based composite have never been the issue.

The main objective of this study is to evaluate the performance of a cement-based composite under the effect of using waste carpet fiber (polypropylene) and waste glass.

2. EXPERIMENTAL APPROACH

2. 1. Material Specifications

The fibers included in this in this study (table 1) were 4.5 denier monofilament fibers obtained from recycled raw materials that were cut to 6.35 mm in length.

Table 1. Properties of Polypropylene fibers reused in this study

Property	Polypropylene
Unit weight [g/cm3]	0.9 - 0.91
Reaction with water	Hydrophobic
Tensile strength [ksi]	4.5 - 6.0
Elongation at break [%]	100 – 600
Melting point [°C]	175
Thermal conductivity [W/m/K]	0.12

The chemical composition of the reused glass was analyzed using an X-ray microprobe analyzer and listed in table 2 together with that of silica fume and rice husk ash for comparison.

In accordance to ASTM C618, the glass satisfies the basic chemical requirements for a pozzolanic material. However, it dose not meet the optional requirement for the alkali content because of high percentage of Na_2O.

Table 2. Chemical composition of materials

	Content (%)		
Oxide	Glass C	Silica fume	Rice husk ash
SiO_2	72.5	91.1	92.1
Al_2O_3	1.06	1.55	0.41
Fe_2O_3	0.36	2	0.21
CaO	8	2.24	0.41
MgO	4.18	0.6	0.45
Na_2O	13.1	-	0.08
K_2O	0.26	-	2.31
CL	0.05	-	-
SO_3	0.18	0.45	-
L.O.I	-	2.1	-

To satisfy the physical requirements for fineness, the glass has to be grounded to pass a 45μm sieve. This was accomplished by crushing and grinding of glass in the laboratory, and by sieving the ground glass to the desired particle size. To study the particle size effect, two different ground glasses were used, namely:

- Type I: ground glass having particles passing a #80 sieve (180μm);
- Type II: ground glass having particles passing a #200 sieve (75μm).

The particle size distribution for two types of ground glass, silica fume, rice husk ash and ordinary Portland cement were analyzed by laser particle size set and have shown in figure 1. As it can be seen in figure 1 silica fume has the finest particle size. According to ASTM C618, fine ground glasses under 45μm qualify as a pozzolan due to the fine particle size. Moreover glass type I and II respectively have 42% and 70% fine particles smaller than 45μm that causes pozzolanic behaviour and doesn't occur any excessive expansion due to alkali–silica reaction (ASR).

Also standard river sand and Portland cement type1 were used for preparing the specimens.

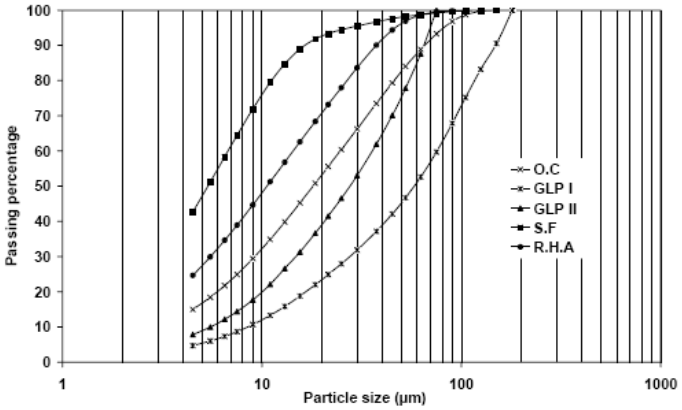

Figure 1. Particle size distribution of ground waste glass type I, II, silica fume, rice husk ash and ordinary cement.

Table 3. Mixture proportions

batch No	sand/c	w/c	Content (by weight)					PP fibers	batch No	sand/c	w/c	Content (by weight)					PP fibers
			O.C	GI	GII	SF	RH	(by volume)				O.C	GI	GII	SF	RH	(by volume)
1	2.25	0.47	100	-	-	-	-	0	11	2.25	0.6	100	-	-	-	-	1
2	2.25	0.47	90	10	-	-	-	0	12	2.25	0.6	90	10	-	-	-	1
3	2.25	0.47	90	-	10	-	-	0	13	2.25	0.6	90	-	10	-	-	1
4	2.25	0.47	90	-	-	10	-	0	14	2.25	0.6	90	-	-	10	-	1
5	2.25	0.47	90	-	-	-	10	0	15	2.25	0.6	90	-	-	-	10	1
6	2.25	0.6	100	-	-	-	-	0.5	16	2.25	0.6	100	-	-	-	-	1.5
7	2.25	0.6	90	10	-	-	-	0.5	17	2.25	0.6	90	10	-	-	-	1.5
8	2.25	0.6	90	-	10	-	-	0.5	18	2.25	0.6	90	-	10	-	-	1.5
9	2.25	0.6	90	-	-	10	-	0.5	19	2.25	0.6	90	-	-	10	-	1.5
10	2.25	0.6	90	-	-	-	10	0.5	20	2.25	0.6	90	-	-	-	10	1.5

2.2. Test Program

For the present study, twenty batches were prepared. Control mixes was designed containing natural sand at a ratio of 2.25:1 to the cement matrix. Concerning %10 of cement weight replaced by the ground waste glass type I and II(GI,GII) , silica fume(SF) and rice husk ash (RH). Meanwhile, modified batches were designed with the same admixtures but reinforced with 0.5%, 1% and 1.5% (by volume) of polypropylene fibers (PP). In the control batches, water to cementitious ratio of 0.47 was used whereas in modified mixes (with different amount of PP fibers) water to cementitious ratio was 0.6. The mortar mixture proportions are represented in table 3.

The strength criteria of mortar specimens and impacts of polypropylene fibers on characteristics of these specimens were evaluated at the age of 7, 28 and 60 days.

In our laboratory, the test program conducted as follows:

1. The fibers were placed in the mixer.
2. Three-quarters of the water was added to the fibers while the mixer was running at 60 rpm; mixing continues for 1 minute.
3. The cement was gradually added while the mixer was still running. After adding the cement, the mixer is allowed to run for two minute to allow the cement to mix with the water.
4. The sand and remaining water were added, and the mixer was allowed to run for another two minutes.

After mixing, the samples were casted into the forms $50 \times 50 \times 50 mm$ for compressive strength and $50 \times 50 \times 200 mm$ for flexural strength. All the moulds were coated with mineral oil to facilitate demoulding. The samples were placed in two layers. Each layer was tamped at least 25 times using a hard rubber mallet. The sample surfaces were finished using a metal spatula. After 24 hours, the specimens were demoulded and cured in water at $20^{\circ} C$.

3. RESULTS AND DESICCATIONS

3.1. Compressive Strength

The variations of compressive strength with age are presented in figure 2. The compressive strength of the composite in comparison with control specimens containing 0% fiber is represented in figure 2.a. A significant decrease in compressive strength can be observed. In view of the above, the lowest decline belongs to the composite containing 10% silica fume (SF) and the highest are related to composites containing 10% glass I (GI) and rice husk ash (RH). The compressive strength of SF specimens is close to target specimens due to the finest particle size and highest pozzolanic behaviour. This is however confirmed according to ASTM C618. Meanwhile, glass type 1(GI) due to coarse size of aggregates exhibit low pozzolanic behavior.

In addition, however the pozzolanic behaviour of rice husk ash in early age is low but by ageing the specimens, this effect will rise significantly.

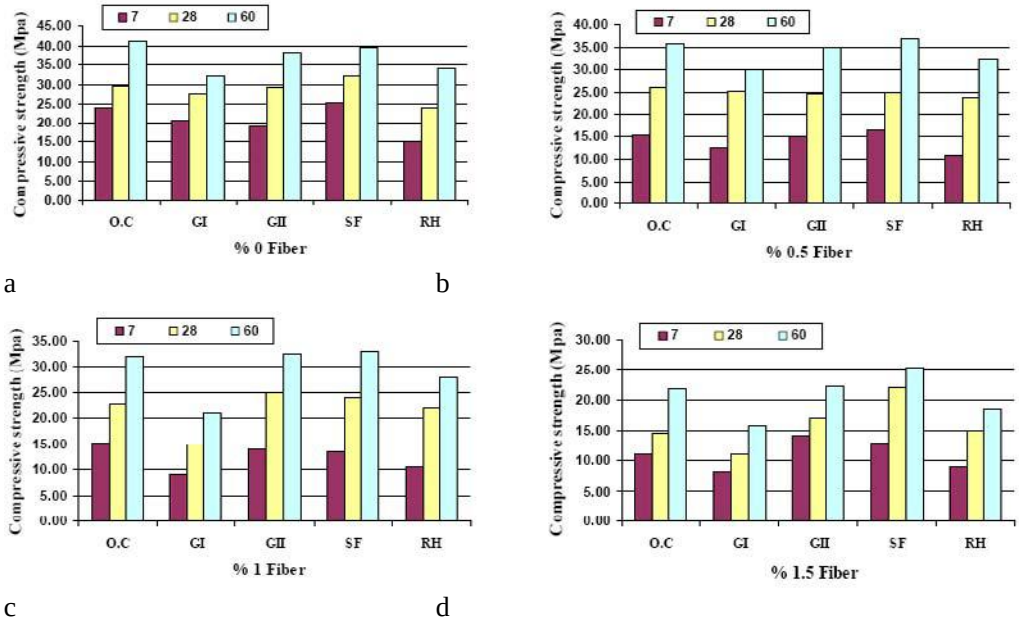

Figure 2. Compressive strength of mortars in different ages.

The variation of compressive strength with age shows a continuous increase by decreasing the amount of polypropylene fibers in matrix (figures 2.b, c and d.). The specimens contain 1.5% PP fiber by volume exhibit a considerable reduction around 50% in compressive strength comparing to target specimen. Although the variation of strength in mortars contained 0.5% PP by volume is not significant. Despite of compressive strength decrement in reinforced matrix contained PP fiber, the specimens which contains silica fume (SF) and PP fiber have shown greater compressive strength than the others. Moreover GII approximately indicates the same results to target specimens.

In view of the above, the replacement SF and GII (in which 70% of fine particles are smaller than 45μm)is directly proportional to their respective pozzolanic activity index values (according to ASTM C618 and C989 and table 2).

3.2. Flexural Strength

The effect of fiber volume fraction, and the age of the mortar matrix on the flexural strength are represented in figure 3.

In all cases, by increasing the amount of fiber in matrix and ageing of specimens, the flexural strength tends to increase.

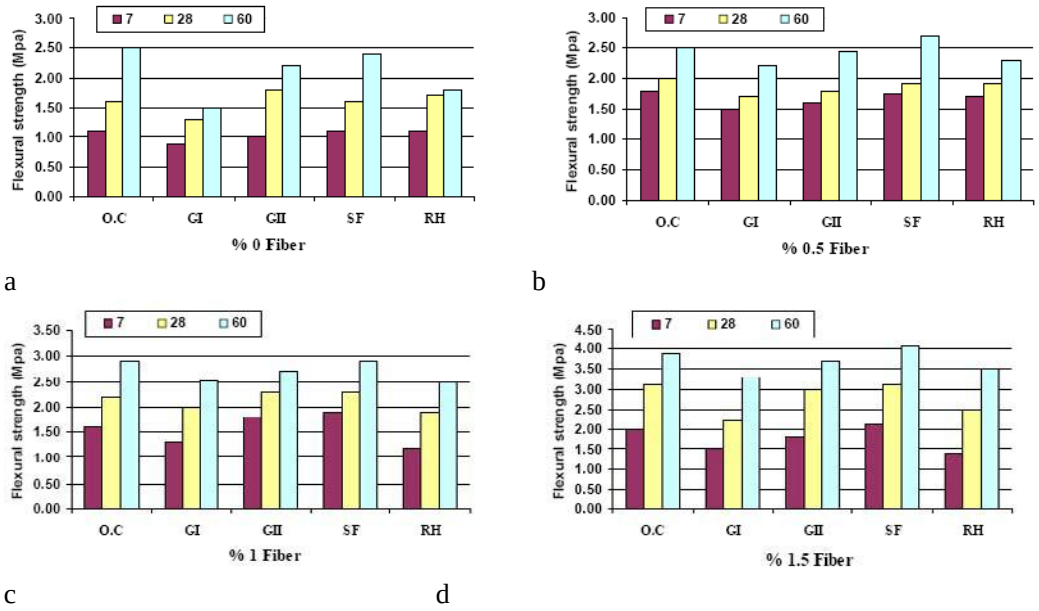

Figure 3. Flexural strength of mortars in different ages.

In view of the above, the highest flexural strength between control specimens belong to O.C, 10% SF and 10% GII replacement in cement which is relevant to pozzolanic activity which mentioned before.

The flexural strength of specimens contained 0.5% PP fiber doesn't show considerable increment. Nevertheless, in mixes contained 1% and 1.5% PP fibers, represent a relative increment in flexural strength.

It is also observed that the lowest strength is related to GI in all mixes due to course particle size and low pozzolanic behaviour.

3.3. Flexural Toughness

Toughness is defined as the ability of materials to sustain load after initial cracking and is measured as the total strain experienced at failure. Upon cracking, fibers are able to bridge the initial crack and hold the crack together until the fibers either pull-out from the matrix (in early age) or fracture that say flexural toughness.

Figure 4 represents typical load-deflection responses of plain matrix and mixtures contained 0.5%, 1%, and 1.5% fibers.

For plain mortars, the behaviour was in a brittle manner. When the strain energy was high enough to cause the crack to self-propagate, fracture occurred almost while the peak load was reached (this is due to the tremendous amount of energy being released). For fiber reinforced mixes, the fiber bridging effect helped to control the rate of energy release. Thus, fibers still can carry load even after the peak. With the effect of fibers bridging across the crack surface, fiber was able to maintain the load carrying ability even after the mortar had been cracked. According to ASTM C1018 [11], toughness or energy absorption defined as the area under the load-deflection curve from crack point to 1/150 of span.

Results indicate that, by increasing the amount of fiber in matrix flexural toughness rise significantly.

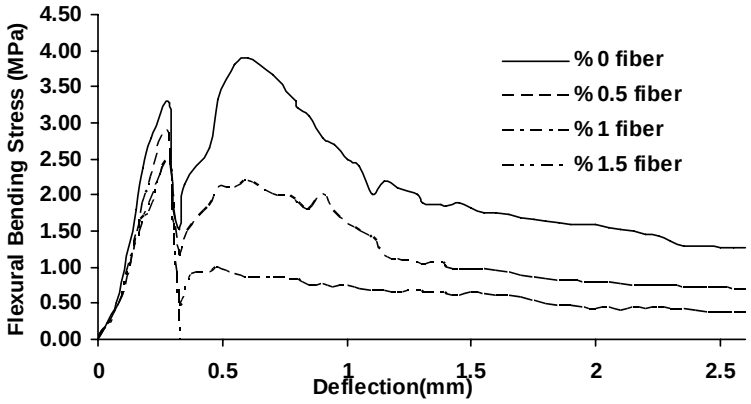

Figure 4. Load-Deflection Response of plain and polypropylene fiber reinforced mortar.

3.4. Water Absorption

Water absorption of specimens is measured and evaluated in table 4 according to ASTM C642.

In general, the incorporation of SF improves the water absorption properties of the material because of the reduction of permeable voids. The same behavior was reported by Aguilar et al. [5] when they studied steel and nylon fiber reinforced Portland cement matrices with additions of SF and GGBS (granulated blast furnace).

Table 4. Water absorption of all mixes

batch No	Water absorption	batch No	Water absorption	batch No	Water absorption	batch No	Water absorption
1	5.83	6	7.10	11	8.50	16	10.80
2	5.30	7	7.42	12	8.80	17	10.52
3	5.16	8	6.59	13	8.12	18	10.22
4	4.36	9	5.42	14	6.37	19	8.15
5	4.77	10	5.30	15	6.79	20	8.42

A reduction in water absorption is expected when a pozzolanic material is added to the matrix. SF addition had the greatest effect, followed by RH and GII addition but GI doesn't show a significant effect on water absorption. This is due to particle size and then, pozzolanic activity of materials.

This explains that by increasing the fiber percentage in the matrix of mortars, water absorption will increase, as well.

4. CONCLUSION

This research study proves the feasibility of the use of glass as aggregates replacement and PP fibers for composite reinforcement. Based on the experimental results of this investigation the following conclusion can be drawn:

- Application of fibers in matrix causes the noticeable reduction in compressive strength and negligible rise in flexural strength.
- Mixture of cement based composite with GII and SF containing different percentage of fibers shown close properties to target specimens. So results show the great possibility of usage of ground glass and silica fume in mortars as a replacement in cement.
- Increasing the fibers in matrix causes low compressive strength, but it increases the flexural toughness substantially. In fact the ability for absorbing the energy rises up.
- Water absorption will decrease by addition of pozzolanic materials in to the matrix because of fine particle size and covering the permeable voids.

REFERENCES

[1] Bentur A, Mindess S. Fiber reinforced cementitious on durability of concrete. Barking: Elsevier, 1990.

[2] Balaguru PN, Shah SP. Fiber reinforced cement composites. New York: McGraw-Hill, Inc, 1992:367p.

[3] Duckett, K., "Olefin Fiber" and "Nylon Fibers", Project: Textile Science 526 - Nonwovens Science and Technology II, (http://trcs.he.utk.edu/textile/nonwovens/), Fall 1999.

[4] Callister, W.D., Material Science and Engineering - An Introduction, 4th ed., John Wiley & Sons, New York, 1997.

[5] Aguilar MTP, Gomes AM, Cetlin PR, Friche GHS. Proc. II International Conference on High Performance Concrete, ramado, Brazil, 1999. SP58

[6] S. Kumar, M. B. Polk, and Y. Wang, Fundamental studies on the utilization of carpet waste, presented at the SMART (Secondary Materials & Recycled Textiles, An International Association) 1994 Mid-Year Conference July, 1994, Atlanta, GA.

[7] Y. Wang, S. Kumar, and M.B. Polk, Fundamental studies on the utilization of carpet waste, presented at The Fiber Society Spring Technical Conference, May, 1994, Annapolis, MD.

[8] Y. Wang, B.S. Cho, and A. H. Zureick, Fiber Reinforced Concrete Using Recycled Carpet Industrial Waste and Its Potential Use in Highway Construction, in Proceedings of the Symposium on Recovery & Effective Reuse of Discarded Materials & By-Products for Construction of Highway Facilities, U.S. Department of ransportation, October, 1993, Denver, CO.

[9] Y. Wang, A. Zureick, B.S. Cho, D. Scott, “Properties of Fiber Reinforced Concrete Using Recycled Fibers from Carpet Industrial Waste”, Journal of Materials Science, in print, 1994.

[10] R. K. Datta, M. B. Polk, and S. Kumar, Reactive Extrusion of Polypropylene and Nylon, Polymer-Plastics Technology and Engineering, in print, 1994.

[11] ASTM C 1018. Test method for flexural toughness and first crack strength of fiber reinforced concrete using beam with third-point loading. Annual Book of ASTM Standards, 04.02, 1988:491]496